

Modeling and Design of Integrated Optical
Microresonator with Rectangular Cavity
Shapes

Didit Yudistira

June, 2003

Contents

1	Introduction	3
1.1	Background	3
1.2	Objective	4
1.3	Notation and Assumptions	5
1.4	Organisation of the thesis	5
2	Coupled-mode theory modeling	7
2.1	Codirectional Propagation along Parallel Multimode Waveguides	8
2.2	Reflector-Bragg Waveguide	14
2.3	CMT Microresonator Model	22
2.3.1	Resonant State	24
3	Applications of the Formulation	28
3.1	Structural parameters	29
3.1.1	Port waveguides	29
3.1.2	Bragg-grating	30
3.1.3	Cavity waveguide	31
3.2	Simulation results	34
3.2.1	Symmetric Bragg-reflectors	34
3.2.2	Nonsymmetric Bragg-reflectors	40
3.2.3	Filter simulations	41

<i>CONTENTS</i>	2
4 Conclusions and remarks	49
A Cholesky Decomposition	51
B Matlab Code	53
Bibliography	61
Acknowledgment	64

Chapter 1

Introduction

1.1 Background

In the past years, the technological progress in the field of integrated optics has opened up possibilities for the realisation of optical devices with higher complexity and integration density. In applications especially in optical communications, optical wavelength division multiplexing (WDM) is a major objective of the current research efforts. Some promising device concepts have been investigated and developed using microresonator elements as basic building blocks [11]. The typical microresonator device consists of two parallel straight waveguides and a small optical cavity placed between these two in which the waveguides function as input and output ports. The characteristic spectral response enables the design of microresonator devices with a variety of functionalities, e.g. filtering, switching, routing, or modulation.

In the past few years, in particular microresonator with cylindrical [10] cavity shapes have been investigated. Rectangular cavity shapes have also attracted some interests [14, 15, 12], but only quite recently. However in applications the conventional form of rectangular cavity shapes requires an extremely high refractive index contrast for the total reflection at facets of the cavity segment [7]. In order to deal with this problem, a way out is found by replacing the waveguide facets by Bragg reflectors [8]. This leads to device similar to the well known Fabry-Perot resonator concept. The

devices itself is then called a grating assisted rectangular optical microresonator.

At least in a two dimensional setting the structures can be analysed quite rigorously by means of finite differences, bidirectional eigenmode propagation (BEP), and mode expansions. Because of rigorousness, these approaches give only little insight into the design principles of the structure. For this purpose in this thesis we will analyse the structure by means of coupled-mode theory (CMT)[5].

In this analytical approximate approach, the total field of the coupled waveguides is expressed as a linear combination of the modal fields supported by the individual waveguides. The power transfer between the propagating modes is described by the coupled-mode equations for the modal amplitudes. Coupling effects are characterised only by the coupling coefficients and therefore it is easily applied when the number of waveguides increases. In particular the coupled-mode theory allows to consider the cavity separated from the port waveguide and grating segment. The formulation resembles that given in Ref. [13] for the unidirectional light propagation along a three waveguide coupler where forward and backward traveling field are considered simultaneously.

1.2 Objective

As stated generally in the previous section the purpose of this thesis is to investigate the grating assisted rectangular microresonators using coupled-mode theory as a basic simulation tool [5]. The coupled-mode technique has occupied an important place in applied mathematics and physics because the perturbational expansions are useful for a qualitative as well as quantitative approximation representation of the solution. The investigation is limited to the 2D problem and the resonant wavelength interests elsewhere around $\lambda_0 = 1.55 \mu\text{m}$. The wavelength range is of interest to be in between $1.5 \mu\text{m}$ and $1.6 \mu\text{m}$. The present thesis uses a coupled-mode formulation based on perturbation techniques and a assumption that the individual waveguide modes are nonorthogonal. The basic idea of the formulation was originally presented by Hammer [6] for rectangular microresonators without Bragg-reflectors. Here, we will do calculations for devices with

Bragg-reflectors. We will apply this formulation to several specified configurations of the microresonators. The validity of the formulation will be confirmed by comparing with more accurate numerical simulations with a commercial tool *Olympios* [3] based on bidirectional eigenmode propagation (BEP).

1.3 Notation and Assumptions

The optical electromagnetic field consists of electric part $\mathcal{E}(x, z, t)$ and magnetic part $\mathcal{H}(x, z, t)$. Note that these are vector fields, which means that at any point in space (x, z) and at any time t , both \mathcal{E} and \mathcal{H} are (where we adopt common complex notation) vectors that can differ at every position, and can point in any direction. In this thesis, time harmonic electromagnetic waves are investigated. A time dependence of a monochromatic wave $e^{j\omega t}$ is always assumed with $j = \sqrt{-1}$. The expression is usually omitted. The constant angular frequency $\omega = kc = 2\pi c/\lambda$ is related to the vacuum wavenumber k , to the vacuum speed of light c , and to the vacuum wavelength λ . All dielectrics under consideration are linear, isotropic, lossless media, and the permeability μ of free space is assumed. When applying CMT, we shall deal with only guided mode waves propagating along the waveguide structures, and in that case the radiative parts of the field are ignored. It is customary to normalise the mode profiles such that the arbitrary normalisation constant is equal to 1, and can therefore be omitted; so that any modal field \mathbf{E}_i and \mathbf{H}_i will always be normalised as

$$\int_{A_\infty} [\mathbf{E}_i \times \mathbf{H}_i] \cdot \mathbf{z} dA = 1$$

In all simulations we assume that the fields TE polarised.

1.4 Organisation of the thesis

This thesis is organised as follows. This Chapter 1 gives an introduction. It shows the backgrounds and objective of our study. The notation rules and assumptions are also presented in this chapter.

In Chapter 2, the coupled-mode theory modeling for a grating assisted rectangular microresonator problem is explained in detail. We will start with the analysis of codirectional propagation in parallel multimode waveguides and it is followed by the analysis of Bragg-reflectors with so-called contradi-rectional coupled-mode theory. In Section 2.3 these analyses are combined and yield a single coupled-mode formulation for the corresponding problem. In a subsection of Section 2.3, we also explain in detail about the characteristics of resonance in the cavity.

The application of the coupled-mode formulation will be presented in Chapter 3. The first application considered in Section 3.1 is an analysis of the structural parameters of the device and the procedure to select them. Next, the implementation of CMT to three different configuration settings of the resonator is presented. We verify the CMT results by comparison with rigorous numerical computations (BEP) with *Olympios*.

In Chapter 4, the results obtained throughout this study are briefly summarised, and also some remarks regarding the performance of CMT compared to *Olympios* in terms of computation times and computer efficiency are given.

Chapter 2

Coupled-mode theory modeling

The geometry of the grating assisted rectangular microresonator is shown in Fig. 2.1. The device consists of two parallel waveguide cores of width

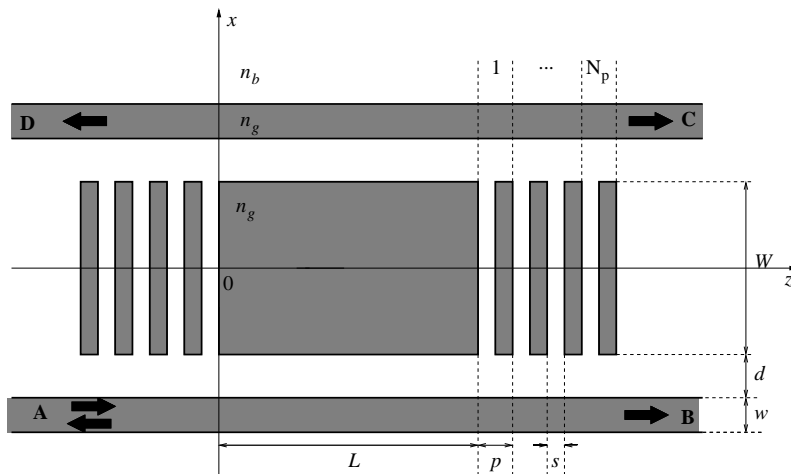


Figure 2.1: Schematic of a grating assisted rectangular microresonator

w , the port waveguides which are coupled by a cavity waveguide of width W and length L , separated by gaps d . In addition gratings with N_p periods of length p with a spacing s enclose the cavity. The refractive index of

guiding regions is denoted by n_g and n_b denotes the refractive index of the background medium. Capital letters A to B denote the input and output ports.

From this figure we see that the problem for the entire resonator indeed becomes complicated. Rather than doing the calculation in one time for the whole structure, in this thesis we propose to investigate the structure partly by splitting the problem in two separated problems, namely the cavity segment and the grating problem (left and right grating). Thus we will get two sets of coupled-mode equations, one for the cavity segment and another one for the grating part, which can be solved independently. After that we combine the two solutions to a complete solution of the resonator problem. For simplification, when deriving the coupled-mode theory for the grating part, we neglect the presence of the port waveguides. This simplification leads to a model of ordinary contradirectional coupling for the grating problem. An illustration of the splitted structure is given in Fig. (2.2).

The problems are treated as follows. We start with a CMT model for the cavity segment, continue with a model for the grating structure, and finally we combine them.

2.1 Codirectional Propagation along Parallel Multimode Waveguides

The region $0 < z < L$ of the microresonator can be regarded as a symmetrical directional coupler which consists of three parallel waveguides, where WG I and WG II are called the port waveguides, and WG III is called the cavity waveguide, as illustrated by Fig. (2.3). In an isolated condition, the port waveguides with thickness w are supposed to support only one mode, whereas the cavity with thickness W may support more than one mode. The basis fields are given by the electric part $\mathbf{E}_k = (0, E_{k,y}, 0)$ and magnetic part $\mathbf{H}_k = (H_{k,x}, 0, jH_{k,z})$ of the mode profile, with real components $E_{k,x}, \dots, H_{k,z}$ depending on the transverse coordinates only. By solving Maxwell equations, the modal fields of the isolated waveguides are given by:

$$\mathcal{E}_k^+(x, z) = \mathbf{E}_k^+(x) \exp[-j\beta_k z],$$

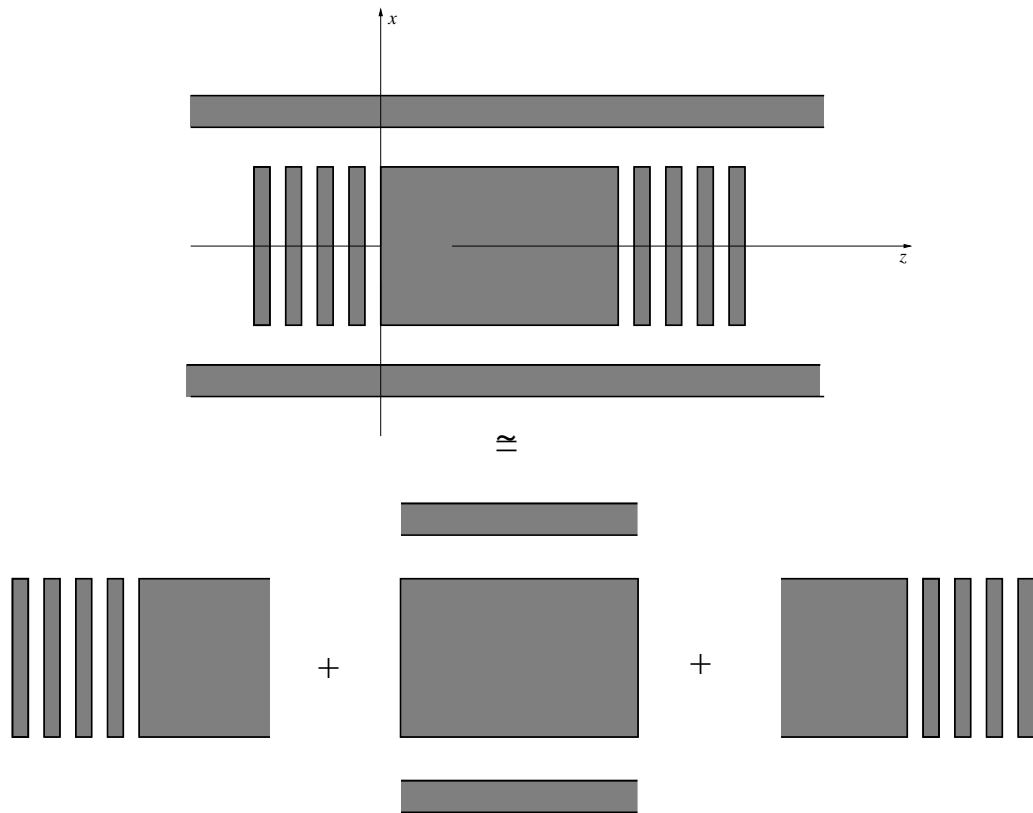


Figure 2.2: The illustration of the approximated model of the grating assisted rectangular microresonator

$$\mathcal{H}_k^+(x, z) = \mathbf{H}_k^+(x) \exp[-j\beta_k z] \quad (2.1)$$

for the forward propagating fields with $k = \text{I, II, III}$ indicating the waveguide. Based on inversion symmetry in the $-z$ direction, the following set of fields will also be solutions to the Maxwell equations [4]

$$\begin{aligned} \mathcal{E}_k^-(x, z) &= \mathbf{E}_k^-(x) \exp[j\beta_k z] \\ \mathcal{H}_k^-(x, z) &= \mathbf{H}_k^-(x) \exp[j\beta_k z], \end{aligned} \quad (2.2)$$

where the basis fields for forward propagating modes are given by the electric part $\mathbf{E}_k^+ = (0, E_{k,y}, 0)$, and the magnetic part $\mathbf{H}_k^+ = (H_{k,x}, 0, jH_{k,z})$, while the basis fields for backward propagating fields are given by $\mathbf{E}_k^- = (0, E_{k,y}, 0)$ and $\mathbf{H}_k^- = (-H_{k,x}, 0, jH_{k,z})$. With the convention $\mathbf{E}_k^+ = \mathbf{E}_k^- = \mathbf{E}_k$ and $\mathbf{H}_k^+ = \mathbf{H}_k^-$. In the two sets of solutions above, β_k is a positive number which denotes the propagation constant of mode k at frequency ω corresponding to wavelength λ in vacuum.

In this section, we derive a CMT of the problem by considering the forward

Figure 2.3: Left: the cavity segment. Right: transverse refractive-index variations $n_{\text{I}}(x), n_{\text{II}}(x), n_{\text{III}}(x)$, and $N(x)$ of WGI, WGII, and WGIII and the cavity segment, respectively.

and the backward propagating fields separately. The forward and backward propagating optical electromagnetic fields in the cavity segment are assumed to be superpositions:

$$\begin{pmatrix} \mathcal{E} \\ \mathcal{H} \end{pmatrix}^+(x, z) = \sum_i F_i(z) \begin{pmatrix} \mathbf{E} \\ \mathbf{H} \end{pmatrix}_i^+, \quad (2.3)$$

$$\begin{pmatrix} \mathcal{E} \\ \mathcal{H} \end{pmatrix}^-(x, z) = \sum_i B_i(z) \begin{pmatrix} \mathbf{E} \\ \mathbf{H} \end{pmatrix}_i^- \quad (2.4)$$

of the single modes. Here $F_i(z)$ and $B_i(z)$ denote the modal amplitudes of the fields propagating in the $+z$ and $-z$ direction, respectively. The following derivation is based on the forward propagating fields. The same procedure will be used for the backward propagating field.

From Maxwell equations, the following reciprocity identity can be derived straight forward [16].

$$\operatorname{div}((\mathcal{E}_k^+)^* \times \mathcal{H}^+ - (\mathcal{H}_k^+)^* \times \mathcal{E}^+) = -j\omega\epsilon_o(N^2 - n_k^2)(\mathcal{E}_k^+)^* \mathcal{E}^+ \quad (2.5)$$

Substituting Eq. (2.3) into the reciprocity relation Eq. (2.5). That yields

$$\sum_i M_{ki}^+ (\partial_z F_i(z) + j\beta_k F_i(z)) = -j \sum_i (K_{ki}^+)^{\mathbf{I}} F_i(z) \quad (2.6)$$

with M_{ki}^+ is given by

$$M_{ki}^+ = \frac{1}{4} \int_{-\infty}^{\infty} ((\mathbf{E}_k^+)^* \times \mathbf{H}_i^+ + \mathbf{E}_i^+ \times (\mathbf{H}_k^+)^*) \cdot \mathbf{z} dx, \quad (2.7)$$

and $(K_{ki}^+)^{\mathbf{I}}$ is given by

$$(K_{ki}^+)^{\mathbf{I}} = \frac{1}{4} \omega \epsilon_o \int_{-\infty}^{\infty} (N^2 - n_k^2) (\mathbf{E}_k^+)^* \cdot \mathbf{E}_i^+ dx. \quad (2.8)$$

Due to the fact that $\mathbf{E}_k^+ = \mathbf{E}_k$ and $\mathbf{H}_k^+ = \mathbf{H}_k$, furthermore the superscript $+$ can be omitted.

We can invoke the reciprocity theorem a second time, now in the form

$$\operatorname{div}(\mathcal{E}_k^* \times \mathcal{H}_i - \mathcal{H}_k^* \times \mathcal{E}_i) = -j\omega\epsilon_0(n_i^2 - n_k^2)(\mathcal{E}_k)^* \cdot \mathcal{E}_i. \quad (2.9)$$

Substituting Eq. (2.1) into Eq. (2.9), and inserting K_{ki}^{II} yields

$$M_{ki}(\beta_i - \beta_k) = K_{ki}^{\text{I}} - K_{ki}^{\text{II}}, \quad (2.10)$$

where K_{ki}^{II} is given by

$$K_{ki}^{\text{II}} = \frac{1}{4}\omega\epsilon_o \int_{-\infty}^{\infty} (n_i^2 - n_k^2)(\mathbf{E}_k)^* \cdot \mathbf{E}_i dx \quad (2.11)$$

If β_k and K_{ki}^{I} in Eq. (2.6) are replaced by Eq. (2.10), that leads to the following equation

$$\sum_i M_{ki}(\partial_z F_i(z) + j\beta_i F_i(z)) = -j \sum_i K_{ki}^{\text{II}} F_i(z). \quad (2.12)$$

Combination of Eq. (2.6) and Eq. (2.12) yields the coupled-mode equation

$$\sum_i M_{ki} \partial_z F_i = -\frac{j}{2} \sum_i M_{ki}(\beta_k + \beta_i) F_i - j \sum_i \tilde{K}_{ki} F_i \quad (2.13)$$

where the coupling coefficients \tilde{K}_{ki} are defined by

$$\tilde{K}_{ki} = \frac{1}{8}\omega\epsilon_o \int_{-\infty}^{\infty} (2N^2 - (n_k^2 + n_i^2)) \mathbf{E}_k^* \cdot \mathbf{E}_i dx \quad (2.14)$$

In matrix form, Eq. (2.13) can be written as

$$\mathbf{S} \partial_z \mathbf{F} = -j(\mathbf{Q} + \mathbf{K}) \mathbf{F} \quad (2.15)$$

with real symmetric matrices $\mathbf{S} = (M_{ki})$, $\mathbf{Q} = (M_{ki}(\beta_i + \beta_k)/2)$, and Hermitian $\mathbf{K} = (\tilde{K}_{ki})$ due to the lossless materials.

The solution of Eq. (2.15) can be found by taking the particular ansatz [6]:

$$\mathbf{F}(z) = \sum_s f^s \mathbf{a}^s \exp(-j\beta^s z) \quad (2.16)$$

where in this equation β^s are the the so-called supermode propagation constants and \mathbf{a}^s are the corresponding amplitude vectors . If we substitute this ansatz into Eq. (2.15), it leads to the generalised eigenvalue problem (EVP)

$$(\mathbf{Q} + \mathbf{K})\mathbf{a}^s = \beta^s \mathbf{S}\mathbf{a}^s \quad (2.17)$$

with vectors \mathbf{a}^s satisfying the orthogonality properties $(\mathbf{a}^r)^T \mathbf{S}\mathbf{a}^s = \delta_{rs}$, where δ_{rs} is the Kronecker delta, $\delta_{rr} = 1$ and 0 otherwise . Eq. (2.17) can be solved with Cholesky decomposition by splitting the matrix as $\mathbf{S} = \mathbf{C}^T \mathbf{C}$ to find the supermode propagating coefficients β^s and the vectors \mathbf{a}^s (see Appendix A). The coefficients f^s are defined as $f^s = (\mathbf{a}^s)^T \mathbf{S}\mathbf{F}(0)$ such that the general solution of Eq. (2.15) for the forward propagating along the segment $0 < z < L$ can be written as

$$\mathbf{F}(L) = \mathbf{T}(L)\mathbf{F}(0) \quad (2.18)$$

with

$$\mathbf{T}(L) = \left(\sum_s \exp(-j\beta^s L) \mathbf{a}^s (\mathbf{a}^s)^T \right) \mathbf{S} \quad (2.19)$$

The same procedure is carried out for the backward propagating fields, yielding the general solution :

$$\mathbf{B}(0) = \mathbf{T}(L)\mathbf{B}(L). \quad (2.20)$$

This equation describes the fields which propagate along the cavity segment from $z = L$ to $z = 0$.

2.2 Reflector-Bragg Waveguide

Fig. (2.4) sketches the geometry of the Bragg-reflector structure which is to be investigated. The refractive index profile of the structure is shown in Fig. (2.5b). The grating can be seen as a perturbed structure of the unperturbed one that is shown Fig. (2.5). When the medium is lossless and translational invariant in the z -direction, we know that the field solutions defined by the width W of unperturbed structure of the form given by Eq. (2.1) exist that correspond to fields propagating in the $+z$ direction and Eq. (2.2) for the fields propagating in the $-z$ direction.

In this section we formulate Coupled-Mode Equations (CME) of the problem by considering the forward and backward propagating fields simultaneously. Therefore, it is assumed that the mode fields of the perturbed structure are approximated by a weighted sum of the forward and backward propagating fields of the unperturbed one, with z -dependent modal amplitudes:

$$\begin{pmatrix} \mathcal{E} \\ \mathcal{H} \end{pmatrix}(x, z) = \sum_i F_i(z) \begin{pmatrix} \mathbf{E} \\ \mathbf{H} \end{pmatrix}_i^+(x) + \sum_i B_i(z) \begin{pmatrix} \mathbf{E} \\ \mathbf{H} \end{pmatrix}_i^-(x) \quad (2.21)$$

Substituting this trial field into the reciprocity relation

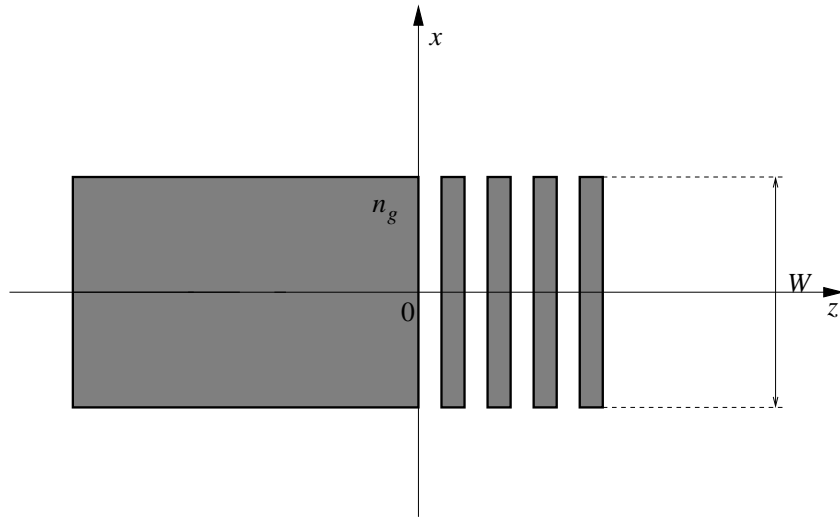


Figure 2.4: Top view of the Bragg grating structure

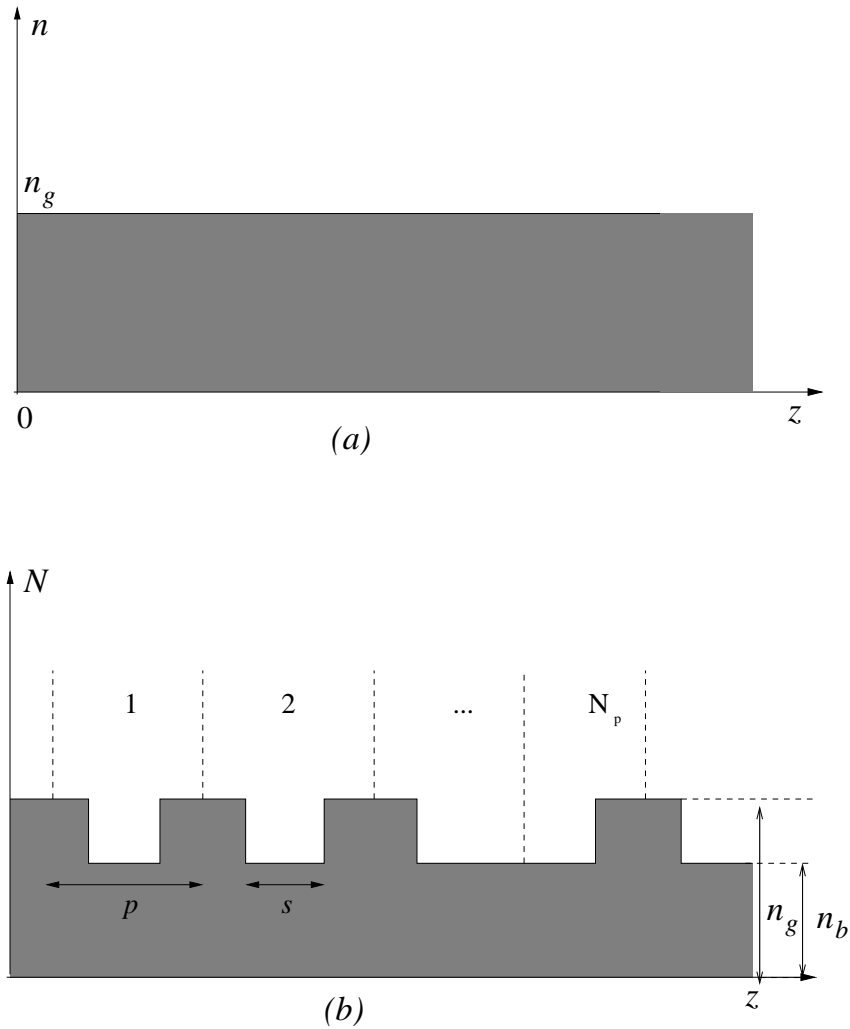


Figure 2.5: (a) and (b) represent the refractive index profiles of the unperturbed and perturbed waveguides along the z -axis, respectively. n_g is the refractive index of the guiding region, n_b is the refractive index of the secondary medium and p is one period length.

$$\operatorname{div}((\mathcal{E}_k^{(+,-)})^* \times \mathcal{H} - (\mathcal{H}_k^{(+,-)})^* \times \mathcal{E}) = -j\omega\epsilon_o(N^2 - n_k^2)(\mathcal{E}_k^{(+,-)})^* \mathcal{E}, \quad (2.22)$$

and integration along the x -axis, after substituting first Eq. (2.1) and secondly Eq. (2.2) into Eq. (2.22), yields to the following set of equations:

$$\sum_i M_{ki}^+ (\partial_z F_i + j\beta_k F_i) = -j \sum_i K_{ki} (F_i + B_i) \quad (2.23)$$

and

$$\sum_i M_{ki}^- (\partial_z B_i - j\beta_k B_i) = -j \sum_i K_{ki} (F_i + B_i). \quad (2.24)$$

In Eq. (2.22) N and n_k associate with the refractive index of perturbed and unperturbed structure, respectively (see Fig. (2.5)). The parameters $M_{ki}^{(+,-)}$ are the power coupling coefficients, where M_{ki}^+ is given by Eq. (2.7) and M_{ki}^- is expressed by

$$M_{ki}^- = \frac{1}{4} \int_{-\infty}^{\infty} ((\mathbf{E}_k^-)^* \times \mathbf{H}_i^- + \mathbf{E}_i^- \times (\mathbf{H}_k^-)^*) \cdot \mathbf{z} dx. \quad (2.25)$$

The parameters K_{ki} are the so-called coupling coefficients:

$$K_{ki} = \frac{1}{4} \omega \epsilon_o \int_{-\infty}^{\infty} (N^2 - n_i^2) (\mathbf{E}_k)^* \cdot \mathbf{E}_i dx \quad (2.26)$$

Eqs (2.23) and (2.24) describe the most general case of mode coupling due to (not necessarily) a periodic dielectric perturbation. In practice, often only the coupling between two modes is relevant. Since we are investigating the contra-directional grating-assisted reflector problem, the coupling interests between one mode traveling in positive z -direction and the corresponding mode traveling in the opposite direction. Neglecting the interaction with any of the other modes, the sum in Eqs. (2.23) and (2.24) can be omitted and the equations turn out to be in the form :

$$(\partial_z F + j\beta F) = -j \frac{K(F + B)}{M^+}, \quad (2.27)$$

and

$$(\partial_z B - j\beta B) = -j \frac{K(F + B)}{M^-}. \quad (2.28)$$

Since $\mathbf{E}^+ = \mathbf{E}^- = \mathbf{E}$, the power coupling coefficients then become.

$$M^- = -M^+ = -\frac{\beta}{2\omega\mu_0} \int_{-\infty}^{\infty} |E_y|^2 dx, \quad (2.29)$$

Let us introduce a new parameter κ associated with the coupling coefficient, defined by

$$\kappa(z) = \frac{1}{2} \frac{\omega\epsilon_0 \int_{-\infty}^{\infty} (N^2 - n^2) |E_y|^2 dx}{\frac{\beta}{\omega\mu_0} \int_{-\infty}^{\infty} |E_y|^2 dx}. \quad (2.30)$$

Substitution of Eqs. (2.29) and Eq. (2.30) into Eq. (2.27) and Eq.(2.28) leads to CME, which read in matrix form

$$\frac{\partial}{\partial z} \begin{bmatrix} F \\ B \end{bmatrix} = -j \begin{bmatrix} \beta + \kappa & \kappa \\ -\kappa & -(\beta + \kappa) \end{bmatrix} \begin{bmatrix} F \\ B \end{bmatrix} \quad (2.31)$$

The difficulty of Eq. (2.31) is that the coupling coefficient is still z -dependent in a complicated way, because N is z -dependent. This dependence can be taken out of the coupling coefficient if it is assumed that the perturbation is small and separable into a x - and z -component [2]. For this case, we can write $N(x, z) = n(x) + \Delta n g(x) f(z)$ and

$$n(x) = \begin{cases} n_g & \text{for } -W/2 \leq x \leq W/2 \\ n_b & \text{for } \text{otherwise} \end{cases} \quad (2.32)$$

where $\Delta n g(x) f(z)$ is very small due to the refractive index contrast $\Delta n = n_b - n_g$ assumed to be small. Therefore, the following approximation can now be made:

$$N^2 - n^2 \approx 2n_g \Delta n f(z) g(x) \quad (2.33)$$

where n_g and n_b are the refractive index of the guiding layer and the background, respectively. The function $g(x)$ describes how the refractive index varies along the x -axis and $f(z)$ describes the variation of the perturbation Δn along the z -axis. The variation of the perturbation $f(z)$ is defined by

$$f(z) = \begin{cases} 0, & \text{for } 0 \leq z < (\Lambda - s)/2 \\ 1, & \text{for } (\Lambda - s)/2 \leq z < (\Lambda + s)/2 \\ 0 & \text{for } (\Lambda + s)/2 \leq z < \Lambda \end{cases} \quad (2.34)$$

with periodic extension, and $g(x)$ is given by

$$g(x) = \begin{cases} 1, & \text{for } -W/2 \leq x \leq W/2 \\ 0, & \text{for } \text{otherwise} \end{cases}. \quad (2.35)$$

We substitute Eq. (2.33) into Eq. (2.30) for the coupling coefficient. The result is

$$\kappa(z) = \frac{1}{N_{\text{eff}}} k n_g \Delta n f(z) \frac{\int_{-W/2}^{W/2} |E_y|^2 dx}{\int_{-\infty}^{\infty} |E_y|^2 dx} \quad (2.36)$$

where $N_{\text{eff}} = \beta/k$ is the effective refractive index. Since the perturbation is periodic with period p , the function $f(z)$ can be expanded into a Fourier series as:

$$f(z) = \sum \mathcal{F}_m \exp[jm\mathcal{K}z], \quad \mathcal{K} = \frac{2\pi}{p} \quad (2.37)$$

The Fourier representation of $f(z)$ described by Eq. (2.34) of the grating structure, $0 \leq z \leq L$ and $L = N_{\mathbf{p}}p$, is given by

$$f(z) = \sum_{m \neq 0} -j \frac{1}{2\pi m} (-e^{-j(p+s)\pi m/p} + e^{j(-p+s)\pi m/p}) e^{jm\mathcal{K}z} + \frac{s}{p} \quad (2.38)$$

From Eq. (2.38), we obtain $-j \frac{1}{2\pi m} (-e^{-j(p+s)\pi m/p} + e^{j(-p+s)\pi m/p})$ and $\mathcal{F}_0 = s/p$. By separating the mode amplitudes of the trial functions, $F(z)$ and $B(z)$, into a slowly-varying envelope and a fast-oscillating carrier

$$\begin{aligned} F(z) &= A_1(z) e^{-j\beta z} \\ B(z) &= A_2(z) e^{j\beta z} \end{aligned} \quad (2.39)$$

and substituting this equation and Eq. (2.37) into (2.31), Eq. (2.31) reduces

to

$$\frac{\partial}{\partial z} \begin{bmatrix} A_1 \\ A_2 \end{bmatrix} = -j \begin{bmatrix} \sum_m C_m e^{jm\mathcal{K}z} & \sum_m C_m e^{j(2\beta+m\mathcal{K})z} \\ -\sum_m C_m e^{-j(2\beta-m\mathcal{K})z} & -\sum_m C_m e^{jm\mathcal{K}z} \end{bmatrix} \begin{bmatrix} A_1 \\ A_2 \end{bmatrix} \quad (2.40)$$

These equations describe the coupling between two modes of the unperturbed waveguide, propagating both in $+z$ and $-z$ directions. Most of the terms on the right-hand side oscillate rapidly with z , making a significant power exchange of A_1 and A_2 impossible. There will be a significant power exchange between the two modes, if the exponent terms are close to zero. This condition is known as the phase-matching condition. As a simplification, the sum is restricted to a single term, selected such that the exponent term $2\beta - m\mathcal{K}$ is closest to zero. After applying the phase matching condition, the Eq. (2.40) reduces to

$$\frac{\partial}{\partial z} \begin{bmatrix} A_1 \\ A_2 \end{bmatrix} = -j \begin{bmatrix} C_0 & C_{-m} e^{j\Delta\beta z} \\ -C_m e^{-j\Delta\beta z} & -C_0 \end{bmatrix} \begin{bmatrix} A_1 \\ A_2 \end{bmatrix} \quad (2.41)$$

where $\Delta\beta = 2\beta - m\mathcal{K}$. In Eq. (2.41), C_m , C_{-m} , and C_0 are

$$\begin{aligned} C_{-m} &= \frac{kn_g \Delta n}{N_{\text{eff}}} \mathcal{F}_{-m} \frac{\int_{-W/2}^{W/2} |E_y|^2 dx}{\int_{-\infty}^{\infty} |E_y|^2 dx}, \\ C_m &= \frac{kn_g \Delta n}{N_{\text{eff}}} \mathcal{F}_m \frac{\int_{-W/2}^{W/2} |E_y|^2 dx}{\int_{-\infty}^{\infty} |E_y|^2 dx}, \\ C_0 &= \frac{kn_g \Delta n}{N_{\text{eff}}} \mathcal{F}_0 \frac{\int_{-W/2}^{W/2} |E_y|^2 dx}{\int_{-\infty}^{\infty} |E_y|^2 dx}. \end{aligned} \quad (2.42)$$

Since the matrix in Eq. (2.41) still has a dependence on z , we should transform these equations into a linear set of differential equations with constant coefficients by introducing:

$$\begin{aligned} \tilde{A}_1(z) &\equiv A_1(z) \exp[-\frac{1}{2}j\Delta\beta z], \\ \tilde{A}_2(z) &\equiv A_2(z) \exp[+\frac{1}{2}j\Delta\beta z]. \end{aligned} \quad (2.43)$$

Upon substituting these expressions into Eq. (2.41), the coupled-mode equations become:

$$\frac{\partial}{\partial z} \begin{bmatrix} \tilde{A}_1 \\ \tilde{A}_2 \end{bmatrix} = -j \begin{bmatrix} \frac{1}{2}\Delta\beta + C_0 & C_{-m} \\ -C_m & -\frac{1}{2}\Delta\beta - C_0 \end{bmatrix} \begin{bmatrix} \tilde{A}_1 \\ \tilde{A}_2 \end{bmatrix} \quad (2.44)$$

One can rewrite this equation as:

$$\partial_z \tilde{\mathbf{A}} = -j\mathbf{H}\tilde{\mathbf{A}} \quad (2.45)$$

with $\tilde{\mathbf{A}} = [\tilde{A}_1, \tilde{A}_2]^T$. Since the matrix \mathbf{H} in the equation above is Hermitian because of the lossless system, it can be diagonalised as

$$\mathbf{P}^{-1}\mathbf{H}\mathbf{P} = \mathbf{O}, \quad (2.46)$$

where \mathbf{O} is a diagonal matrix

$$\mathbf{O} = \begin{bmatrix} \lambda_1 & 0 \\ 0 & \lambda_2 \end{bmatrix}.$$

Inserting this in the Eq. (2.45) and pre-multiplying both sides by \mathbf{P}^{-1} we obtain

$$\mathbf{P}^{-1}\partial_z \tilde{\mathbf{A}} = -j\mathbf{O}\mathbf{P}^{-1}\tilde{\mathbf{A}} \quad (2.47)$$

If we define a new vector $\tilde{\mathbf{a}}(z) \equiv \mathbf{P}^{-1}\tilde{\mathbf{A}}(z)$ then the following equation can be derived

$$\partial_z \tilde{\mathbf{a}} = -j\mathbf{O}\tilde{\mathbf{a}} \quad (2.48)$$

the solution to this equation is

$$\tilde{\mathbf{a}}(z) = e^{-j\mathbf{O}z}\tilde{\mathbf{a}}(0) \quad (2.49)$$

the matrix $e^{\mathbf{O}z}$ simply contains the exponentials of the eigenvalues of the matrix \mathbf{H} multiplied by z on its main diagonal. Using the definition of the vectors $\tilde{\mathbf{a}}$ and $\tilde{\mathbf{A}}$ the solution can now be written in terms of the vector $\mathbf{a}(z)$:

$$\mathbf{a}(L) = \mathbf{S}(0, L)\mathbf{a}(0) \quad (2.50)$$

with vector $\mathbf{a}(z) = [F(z), B(z)]^T$. A matrix $\mathbf{S}(0, L)$ appearing in Eq. (2.50) denotes a scattering matrix of p grating periods given by $\mathbf{P}e^{-j\mathbf{O}L}\mathbf{P}^{-1}$. The components of the scattering matrix $\mathbf{S}(0, L)$:

$$\begin{aligned} S_{11} &= \frac{1}{s} [s \cosh sL - j(\frac{\Delta\beta}{2} + C_0) \sinh sL] \exp[+j(\frac{1}{2}\Delta\beta + C_0)L] \exp[-j\beta L], \\ S_{12} &= -\frac{1}{s} C_{-m} \sinh sL \exp[+j(\frac{1}{2}\Delta\beta + C_0)L] \exp[-j\beta L], \\ S_{21} &= -\frac{1}{s} C_m \sinh sL \exp[-j(\frac{1}{2}\Delta\beta + C_0)L] \exp[+j\beta L], \\ S_{22} &= \frac{1}{s} [s \cosh sL + j(\frac{\Delta\beta}{2} + C_0) \sinh sL] \exp[-j(\frac{1}{2}\Delta\beta + C_0)L] \exp[+j\beta L] \end{aligned} \quad (2.51)$$

with:

$$s = \sqrt{C_m C_{-m} - (\frac{\Delta\beta}{2})^2} \quad (2.52)$$

In a contra-directional Bragg grating, a certain amplitude F is prescribed and only the amplitude $B(0)$ of the reflected wave at $z = 0$ is of interest. At the other end of the grating, at $z = L$, the amplitude of the wave traveling in the negative z -direction is zero. Therefore from Eqs. (2.50) and (2.51), we can find the reflection and transmission coefficients:

$$\begin{aligned} r &= -(S_{21}/S_{22}) \\ t &= (S_{11} - S_{12}S_{21}/S_{22})e^{-j\beta L}e^{j\Delta\beta L/2} \end{aligned} \quad (2.53)$$

and then from the expressions for the the reflectance and transmittance: $R = |r|^2$ and $T = |t|^2$ of the grating. Notice that this “reflectance” is actually the power transfer between mode 1 (running in the positive z -direction) to mode 2 (running the negative z -direction) due to coupling between mode 1 and mode 2, where “transmittance” is the power left in mode 1 at the

end of the grating. This reflectance is the important quantity when we are handling the the cavity facet problem in the next section.

2.3 CMT Microresonator Model

Note that the coupled-mode theory is based on basis fields in which the modal fields of the three parallel waveguides in isolated condition are not orthogonal. Theoretical speaking the solution will be perfectly adequate if we remain in this framework that implies the non-unitary matrix $T(L)$. However, if we still keep this viewpoint then we get into difficulties when handling the problem at the facets of the cavity, where the field propagating in the cavity segment is to be connected to the facet model. The facet model is nothing else than the CMT description of the reflector-bragg waveguide that has been derived in previous section.

In order to deal with this problem we have to assume that the problem is defined as two independent problems, where the mode amplitudes that belong to them are orthogonal. That implies that the total power is to be evaluated as the absolute square ($\mathbf{F}^\dagger \mathbf{F}$) of the mode amplitude vectors. Therefore, this setting requires $T(L)$ to be unitary; otherwise the optical power will not be conserved. But $T(L)$ as defined in Eq. (2.19) is not a unitary matrix. Therefore, we should transform the matrix $T(L)$ by splitting the matrix S with the Cholesky factors C . This yields

$$\tilde{T}(L) = CT(L)C^{-1} \quad (2.54)$$

as a replacement for the transmission matrix $T(L)$. In the following we drop the symbol $\tilde{}$ that is a direct consequence of the approximation inherent in coupled-mode ansatz Eq. (2.16). This inconsistency leads to reasonable power transmission curves; the optical power is conserved.

The next step is that we split the expression for the propagation matrix Eq.(2.54) and the amplitude vectors \mathbf{F} and \mathbf{B} as

$$\mathbf{F} = \begin{pmatrix} \mathbf{F}_p \\ \mathbf{F}_c \end{pmatrix}, \quad \mathbf{B} = \begin{pmatrix} \mathbf{B}_p \\ \mathbf{B}_c \end{pmatrix}$$

$$T = \begin{pmatrix} T_{pp} & T_{pc} \\ T_{pc} & T_{cc} \end{pmatrix} \quad (2.55)$$

where the indices p and c denote the quantities related to the port and the cavity, respectively. In this expression we can regard $\mathbf{F}_p(0)$ and $\mathbf{B}_p(L)$ as the amplitudes of the input fields and $\mathbf{F}_p(L)$ and $\mathbf{B}_p(L)$ as the amplitudes of the output fields. The cavity amplitudes F_c and B_c are to be related at the positions $z = 0$ and $z = L$ of the facets of the cavity waveguide. Neglecting completely the presence of the port cores as a rough approximation when handling the cavity facet problem [6], we apply the coupled-mode theory for the reflector-bragg waveguide mentioned in previous section. Restricted to the guided incident and reflected mode in the core layer, the results establish linear relations

$$\begin{aligned} B_c(L) &= rF_c(L) \\ F_c(0) &= rB_c(0) \end{aligned} \quad (2.56)$$

between the mode amplitudes involved in the two independent facet problems at $z = 0$ and $z = L$, where r is a complex number given by Eq. (2.53).

Now we combine the independent expressions Eqs (2.18), (2.20) and (2.55) for the propagation along the cavity segment and Eq. (2.56) for the reflection at the facet. Due to the symmetry of the linear device it is sufficient to consider an input from one side only. If it is supposed that the incoming field is launched from the left $\mathbf{F}_p(0)$ and, there is no incoming field from the right $\mathbf{B}_p(L) = 0$, we obtain

$$\begin{aligned} \mathbf{F}_p(L) &= (\mathbf{T}_{pp} + \mathbf{T}_{pc}r\Omega^{-1}T_{cc}rT_{cc})\mathbf{F}_p(0) \\ \mathbf{B}_p(0) &= \mathbf{T}_{pp}r\Omega^{-1}\mathbf{T}_{cp}\mathbf{F}_p(0) \end{aligned} \quad (2.57)$$

describing the transmission through the device and the reflection caused by the resonator. The amplitudes of the fields inside the cavity are given by

$$F_c(L) = \Omega^{-1}\mathbf{T}_{cp}\mathbf{F}_p(0),$$

$$B_{\mathbf{c}}(0) = \Omega^{-1} T_{\mathbf{cc}r} T_{\mathbf{cp}} \mathbf{F}_{\mathbf{p}}(0), \quad (2.58)$$

and Ω is defined as

$$\Omega = 1 - T_{\mathbf{cc}r} T_{\mathbf{cc}r} \quad (2.59)$$

Let the upper and the lower port waveguides be identified by indices 1 and 2 respectively, with the input field in port A represented by $\mathbf{F}_{\mathbf{p}}(0) = (1, 0)^{\mathbf{T}}$. Then Eq. (2.57) yields :

$$\begin{aligned} P_{\mathbf{A}} &= |B_{\mathbf{p},1}(0)|^2, \\ P_{\mathbf{B}} &= |F_{\mathbf{p},1}(L)|^2, \\ P_{\mathbf{C}} &= |F_{\mathbf{p},2}(L)|^2, \\ P_{\mathbf{D}} &= |B_{\mathbf{p},2}(0)|^2 \end{aligned} \quad (2.60)$$

for the relative amounts of reflected, directly transmitted, and forwards and backwards dropped optical power.

2.3.1 Resonant State

As being stated before in the isolated condition the cavity waveguide supports more than one mode. It means that in principle all cavity modes have to be taken into account in the calculation in order to get the complete solution. However, in practice the phase matching condition, and the resonant states inside the cavity lead to conditions where only one mode in the cavity will play a dominant role.

In a phase-matching state, the maximum fraction of power exchange between port waveguide WGI and the cavity is proportional to $|K_{13}| / (|K_{13}|^2 + (\Delta\beta/2)^2)$ which becomes small if $\Delta\beta \gg |K_{13}|$, where $|K_{13}|$ are the coupling coefficients between port waveguide WGI and the cavity waveguide and $\Delta\beta = \beta_{\mathbf{p}} - \beta_{\mathbf{c}}^{(m)}$. A complete exchange of power is only possible when $\Delta\beta \approx 0$, that is, when phase matching is established [1].

The quantity Ω^{-1} defined by Eq. (2.59) plays a crucial role for the resonant phenomena in the cavity. According to Eq. (2.58), the amplitude of the field at the end of the cavity $F_c(L)$ are excited by mapping the input $F_p(0)$ with T_{cp} and being amplified by the term Ω^{-1} . The amplification factor Ω^{-1} is defined by

$$\Omega^{-1} = \frac{1}{1 + \tilde{r}^4 - 2\tilde{r}^2 \cos(2\phi)} \quad (2.61)$$

with \tilde{r} and ϕ are the absolute value and the phase of $T_{cc}r$, respectively with ϕ is given by $\phi = \varphi - \beta^{(m)}L$ and φ is given by the complex valued amplitude reflection coefficient r of the grating. In a resonant state, the field will be reflected by the right cavity facet and then propagate backward through the cavity. It will be reflected a second time and then be transferred to its original position.

If for instance we take the gap width d between the cavity and the ports that is very large (an isolated cavity), then the cavity entry of the propagation matrix T_{cc} is $\exp(-j\beta^{(m)}L)$, $\beta^{(m)}$ is the propagation constant of the relevant mode m of the cavity. Therefore, in a configuration where the port waveguides are not present, the evaluation of the amplification factors yields a quantitative characterisation of the resonance in the 2D dielectric resonator. This condition shows that the length of cavity L determines the characteristic of the resonance. However, as a matter of fact the presence of the port waveguides also contributes to this characteristic. Simultaneously, the port waveguide configuration determines the strength of the excitation, or whether a resonance appears at all [6].

In isolation condition, the cavity waveguide can viewed as a slab waveguide with its basis modes being the solution of a problem for an ordinary symmetric slab structure. Reflection at the cavity facets preserves that symmetry. Referring to [6] this approximation is adequate for the field inside the cavity.

From the analysis above we find that if a single mode resonance is excited inside the cavity, the resonant and phase matching condition of the cavity are satisfied simultaneously. A single mode then plays a dominant role for the power transfer within the cavity whereas the contributions of the other modes are small compared to this mode, they can be neglected in the

calculation. Hence in the simulation especially when calculating the power transfer from the port waveguide to the the other port through the cavity only one mode of the cavity waveguide with propagation constant β will be employed. Therefore in total there are three modal fields involved: two modes are from the two port waveguides and another one is from the cavity.

Referring to the concept of Fabry-Perot resonator in the rectangular microresonator the resonance phenomenon can be explained as follows. Let us consider the modal field inside the cavity traveling over in one propagation cycle. Let us then assume the field propagating in the positive z -direction with β to the right grating as can be seen in Fig. (2.6).

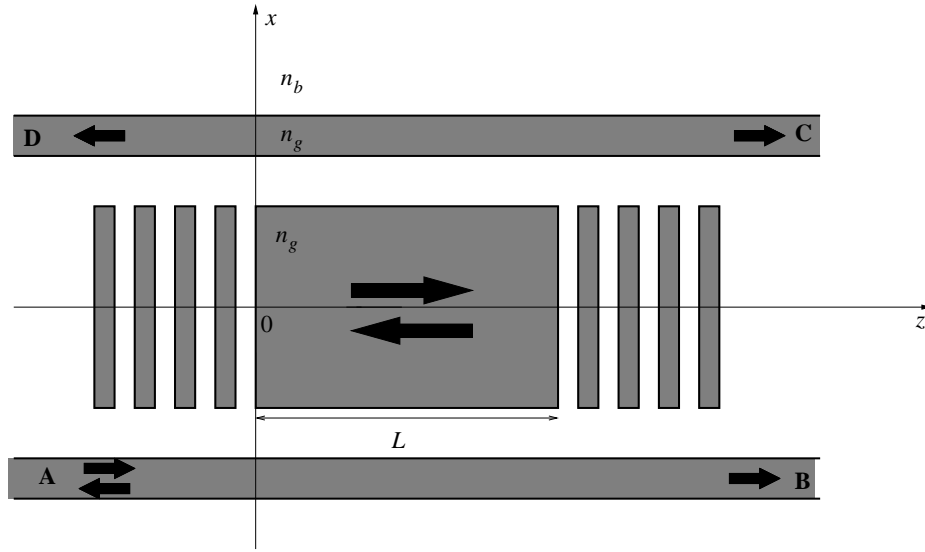


Figure 2.6: Representation of modal field propagating in a grating assisted rectangular microresonator

After one propagation cycle, the field inside the cavity reads

$$E_y(x, z) = \psi(x) \left(1 + |r|^2 e^{-j2\beta L} e^{j2\varphi} \right) \quad (2.62)$$

where $|r|$ and φ are given by the complex valued amplitude reflection coefficient $r = |r| \exp(j\varphi)$ of the grating . Therefore the total power of one propagating cycle take at $z = 0$ is to be

$$|E_y(x, 0)|^2 = |\psi(x)|^2 (1 + 2|r|^2 \cos(2(\beta L - \varphi)) + |r|^4), \quad (2.63)$$

where it will be maximum if $2(\beta L - \varphi) = l2\pi$ or

$$2\beta L = l2\pi + 2\varphi, \quad (2.64)$$

is satisfied with $l = 0, 1, 2, \dots$. The maximum power inside the cavity yields the maximum power coupled to the upper port. Hence Eq. (2.64) is the resonance condition for the rectangular microcavity that has to be fulfilled for the maximum transmission.

Using the relation Eq. (2.64), this is analogous to the common theory of FP resonators. The cavity length have to be chosen according to the following relation:

$$L = (l\pi + \varphi) \frac{\lambda_0}{2\pi N_{\text{eff}}}, \quad (2.65)$$

if a resonance is to be established at wavelength λ_0 , with $N_{\text{eff}} = \beta\lambda_0/2\pi$.

If it is supposed that N_{eff} is wavelength independent and assuming a long cavity $m\phi \gg \varphi$, we obtain the so-called Free Spectral Range (FSR) $\Delta\lambda$ given by

$$\Delta\lambda \approx \frac{\lambda_0}{l} \approx \frac{\lambda_0^2}{2LN_{\text{eff}}}. \quad (2.66)$$

The equation above shows that L or l is to be selected such that there is a chance for pronounced resonances in the window of high Bragg reflectivity around the design wavelength, λ_0 .

Chapter 3

Applications of the Formulation

In the previous chapter the basic simulation tool (CMT) was discussed and the solution of the CME for the present problem was obtained. In the first section of this chapter the geometrical and material parameters of the device will be presented. In determining suitable parameters the formulation given in the previous chapter will be applied. Simulation results for several interesting configurations will be given in the following section. Note that for the geometrical device parameters, we select them such that our device is as small as possible.

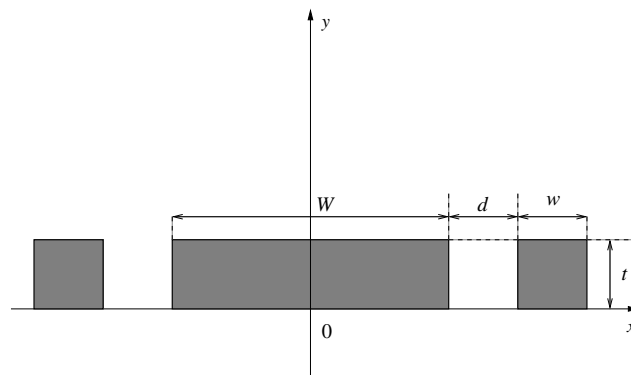


Figure 3.1: Cross section of the realistic device (3D model)

3.1 Structural parameters

As a starting point for the choice of resonator parameters let us consider the medium of the guiding cores and the background medium. Assuming that the hypothetical device will be realised on the the basis of rectangular Si_3N_4 channels with refractive index 1.98 surrounded by a SiO_2 background medium, we fix a common channel thickness of $0.223 \mu\text{m}$ referring to [8]. The illustration of the device can be seen in Fig. (3.1).

Since we are considering a 2D problem, the model has to be transformed to 2D in order apply the presented formulation. After the transformation, the refractive index of the medium is now replaced by an effective index projection of the realistic 3D structure which is determined by solving the eigen mode problem of the ordinary symmetric slab waveguide with the thickness t at the design wavelength $\lambda_0 = 1.55 \mu\text{m}$. It leads to the effective index projection of the realistic 3D structure $n_g = 1.6$ at λ_0 . The refractive index of the background medium remains $n_b = 1.45$. In the 2D investigation, n_b , n_g can be viewed as effective index projection of a 3D device with a cross section shown in Fig. (3.1).

The next step is that we will select suitable geometrical device parameters: the width of the port waveguides w , the width W and the length L of the cavity, and also the grating parameters s and p in such a way that the device will work as required. After all the parameters are fixed, the gap width d should be determined such that on the one hand there is enough power transfer between the port waveguide and the cavity and on the other hand the direct coupling in nonresonant states remains negligible. In this thesis for d we employ a value as proposed by Hammer *et al* [8], where $d = 1.6 \mu\text{m}$.

3.1.1 Port waveguides

Let us consider the port waveguide as a starting point to select the geometrical parameters. The port waveguides have to be designed such that they will support a single mode.

This condition is fulfilled if the width w of the port waveguides is chosen in the range $w \in (0, 1.1458] \mu\text{m}$ calculated at λ_0 . Let us then $w = 1 \mu\text{m}$. With this width we obtain the effective mode index of the port, $N_{\text{eff}} = 1.5404 \mu\text{m}$

at λ_0 . Thus this width number is to be a reference point for the design of the grating and of the cavity waveguide.

3.1.2 Bragg-grating

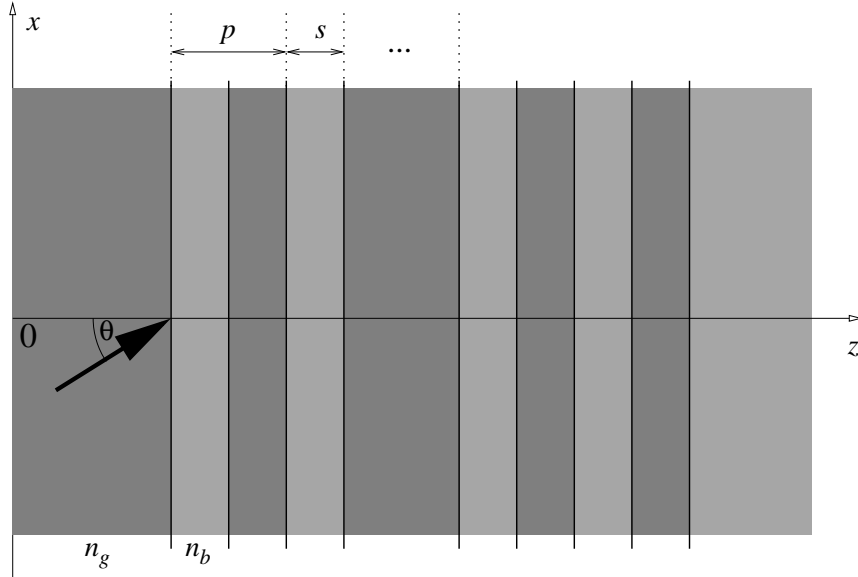


Figure 3.2: A finite periodic multilayer stack

The pronounced resonances require a reflectivity close to unity at the ends of the cavity for the relevant mode that corresponds to the effective mode index of the port waveguides. It is known from previous study [6] that this condition can be satisfied with Bragg-gratings as reflectors put at the cavity facets with suitably selected grating parameters.

The corresponding Bragg-reflector can be constructed on the basis of titled plane wave incidence on a multilayer stack with equivalent refractive index composition (see Fig. (3.2)). We consider an incidence angle θ that corresponds to the angle of the relevant mode in the cavity, where we know that this mode corresponds to the one of the port waveguides with an effective index given by N_{eff} . Using relation $\cos \theta = N_{\text{eff}}/n_g$, we obtain $\theta = 15.69^\circ$.

Optimisation of the layer stack for the present mode angle of 15.69° at λ_0 with the aid of a Transfer Matrix Method (TMM) [19] leads to the grating

parameters $p = 1.538 \mu\text{m}$ and $s = 0.281 \mu\text{m}$, respectively. The reflection will be close to unity if the number of grating periods is selected e.g to be 40 (see. Fig. (3.3)). Although $N_p \geq 40$ will give the same condition, that will increase the size of our device.

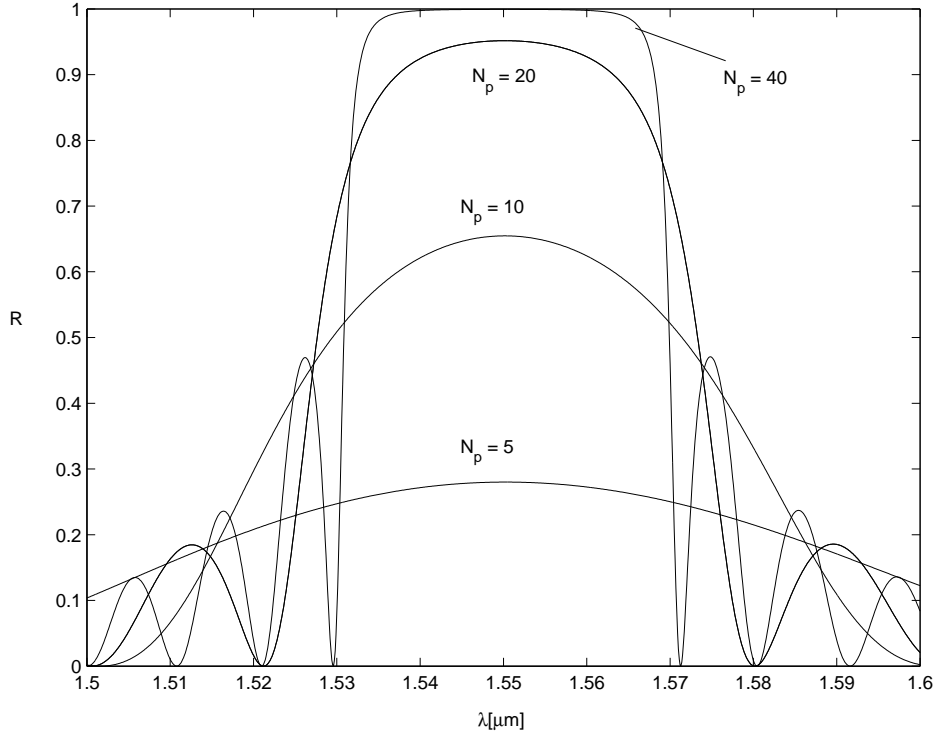


Figure 3.3: Reflectivity R of a multilayer stack for different numbers of grating periods N_p at $\lambda_0 = 1.55 \mu\text{m}$

3.1.3 Cavity waveguide

According to the coupled-mode model provided in previous section for the cavity segment, only one guided mode of the cavity segment is likely to be relevant for a specific standing wave resonance. Due to the phase matching condition that has to be satisfied in the coupling of the fields of the cavity and the port waveguides, the width W of the cavity waveguide has to be adjusted such that the cavity waveguide supports a guided mode that is degenerate with the port fields.

We are then searching W such that one of the effective index mode indices of the cavity is close to $N_{\text{eff}} = 1.5404$. Therefore W will be determined with the aid of the dispersion relation of the symmetric slab waveguide problem (transverse resonance) given by $bW - 2\chi = l\pi$ with $b = k\sqrt{n_g^2 - N_{\text{eff}}^2}$, $\chi = \tan^{-1}(\sqrt{(N_{\text{eff}}^2 - n_b^2)}/b)$; n_g , n_b and N_{eff} are already known. Substituting these parameters into the transverse resonance condition yields

$$W = (1.0 + l1.791) \mu\text{m}. \quad (3.1)$$

Thus the width W has to be selected among the discrete values given by the relation above.

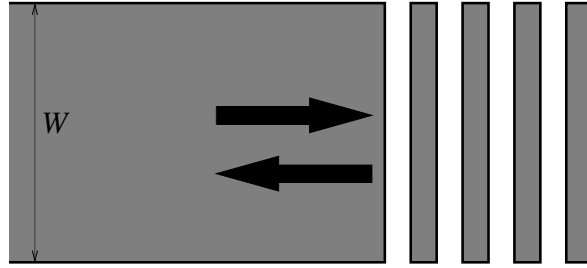


Figure 3.4: The reflection of the mode field by a Bragg-reflector at the end of the cavity waveguide

l	0	1	2	3	4	5
R	0.838	0.898	0.912	0.918	0.922	0.924

Table 3.1: The level of reflectance R in different mode order l

Concerning the reflectivity at the end of the cavity by the grating structure, let us consider Eq. (2.53). In this case, let us then take $N_p = 20$ with a reason that the variation of reflectance R in different cavity width W can be distinguished clearly. By combining Eqs. (2.53) and (3.1) with the aid of the grating parameters s and p and $\beta = kN_{\text{eff}}$ at λ_0 , by CMT computations for a Bragg-reflector as shown in Fig. (3.4) we observed the reflectivity levels as can be seen in Table. (3.1) with the last value already closes to the limiting level of 0.952 of the reflectivity of a plane wave, incident under an angle of 15.69° on laterally unbound multilayer stack. Obviously, the reflectivity is

higher if the fraction of the mode profile that encounters to the corrugation of the Bragg-reflector is larger. Consequently, most of the power can be kept inside the cavity when that condition fulfilled. Therefore a width W corresponding to a higher order mode is preferred. We select $W = 9.955 \mu\text{m}$ which corresponds to the 5th order mode ($l = 5$) for the present simulations. Fig. (3.5) shows that the reflectance spectrum computed by CMT resembles the curve expected from the plane wave model. Actually CMT shows that for $l > 5$ higher reflectivity will be obtained and it is closer to the limiting level. However, it will imply to the size of our device.

Hence a suitable Bragg-reflector indeed can be designed on the basis of the plane wave approach.

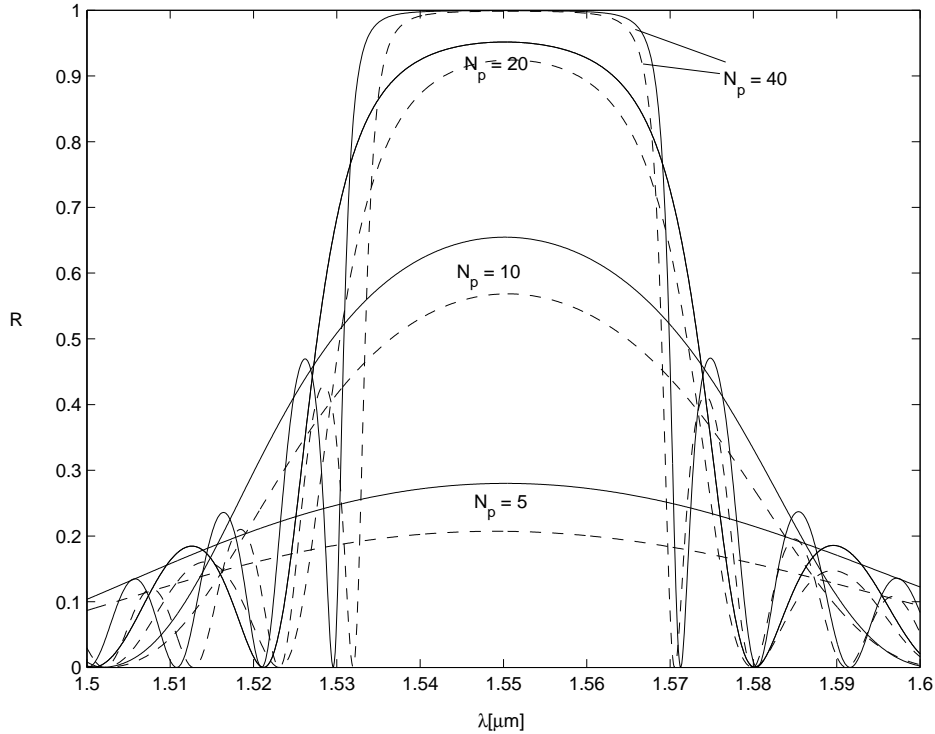


Figure 3.5: Reflectivity R of Bragg-reflectors for the 5th order mode with the selected grating parameters s and p , for different numbers of grating periods N_p . Results calculated using CMT are plotted with dashed lines. The reflectivities of an equivalent multilayer stack for plane wave incidence under the respective mode angle 15.69° are plotted with solid lines.

In determining the cavity length L , we apply the resonance condition given by Eq. (2.65). For the present simulations we refer to [8] with $l = 159$ which corresponds to a cavity length L of about $79.985 \mu\text{m}$.

The design procedure leads to the selected parameters as summarised in Table (3.2). Note that in the following simulation we always keep the pa-

n_g	n_b	$w/\mu\text{m}$	$W/\mu\text{m}$	$L/\mu\text{m}$	$p/\mu\text{m}$	$s/\mu\text{m}$	N_p
1.6	1.45	1	9.955	79.985	1.538	0.281	40

Table 3.2: Material and geometrical parameters

rameters of the cavity and the port waveguides constant, while the grating parameters will be varied for the numerical experiments.

3.2 Simulation results

We have chosen device parameters. In this section we apply the presented coupled-mode formulation. For implementation we use the computing environment *Matlab* [17]. First we consider a resonator with symmetric Bragg-reflectors latter with nonsymmetric reflectors. Finally, we will investigate a filter device.

Alternatively, the devices are simulated with *Olympios* [3]. Here we take the computational windows to be $x \in [-10, 10] \mu\text{m}$ with Perfectly Matched Layers (PML) as boundary conditions (BC) are chosen with a PML thickness of $1 \mu\text{m}$ and a strength of 0.5. The number. BEP modes is set to 128 mode. In the simulations (CMT and *Olympios*) mainly the vacuum wavelength will be varied between $1.5 \mu\text{m}$ to $1.6 \mu\text{m}$ with a stepsize of 0.2 nm and of 0.04 nm for $\lambda \in [1.548, 1.552] \mu\text{m}$.

3.2.1 Symmetric Bragg-reflectors

The input power is launched into the device via the guided mode of port A. As we can see from Fig. (3.6) for most wavelengths the major part of input power is directly transmitted to port B, while at resonance there are some fractions of power transferred into ports A, C, and D as shown by the

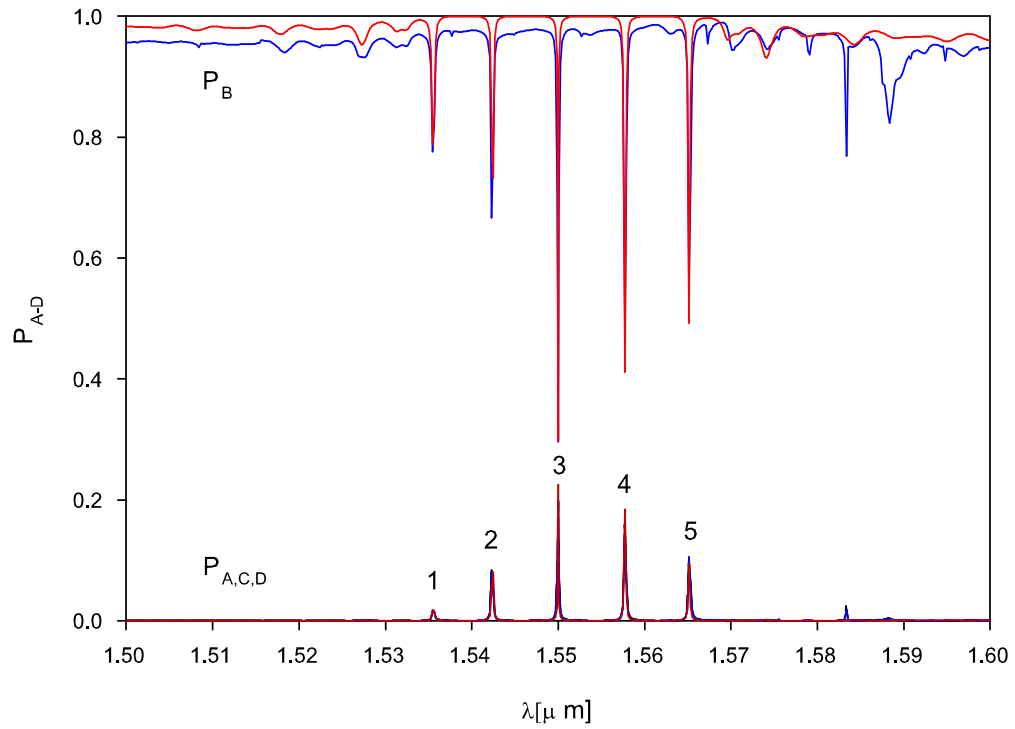


Figure 3.6: Spectral response of resonators with symmetric reflector gratings. P_A to P_D are the relative power fractions that are reflected and transmitted into ports A to D. Red lines shows the simulation results from CMT; *Olympios* results are shown by blue lines.

peaks and dips corresponds to the wavelength. It is observed that the resonant wavelengths are located within stopband region of the grating with $\lambda_0 = 1.55 \mu\text{m}$ as the center of the region. Fig. (3.7) shows the field at resonance at λ_0 . By the simulations of the grating we know that the stopband region given by CMT and *Olympios* is in the wavelength range of $1.532 \mu\text{m}$ to $1.571 \mu\text{m}$.

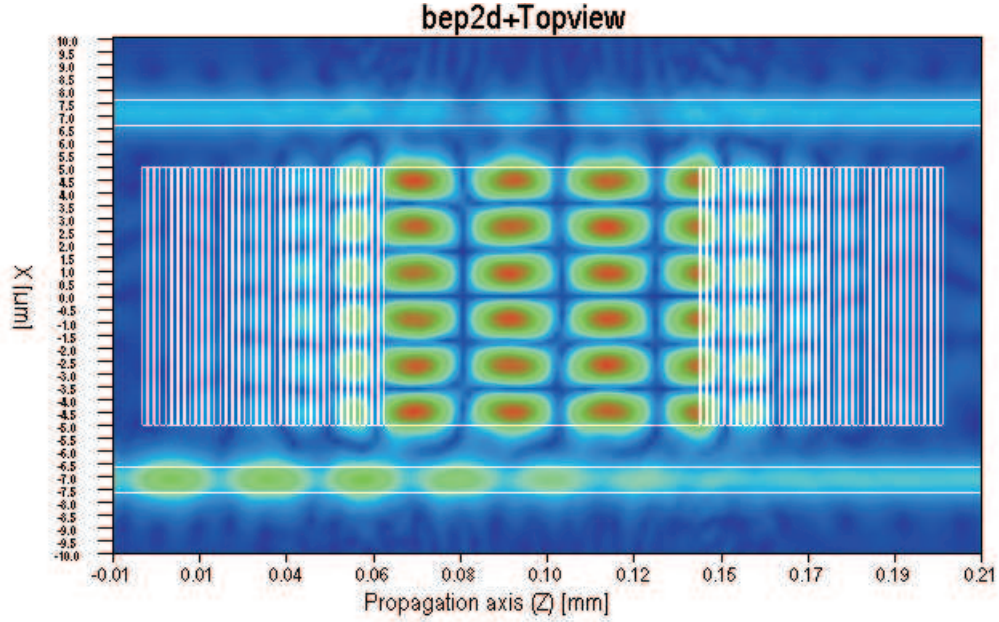


Figure 3.7: Resonant field $|\mathcal{E}_y|^2$ at λ_0 as computed with *Olympios*.

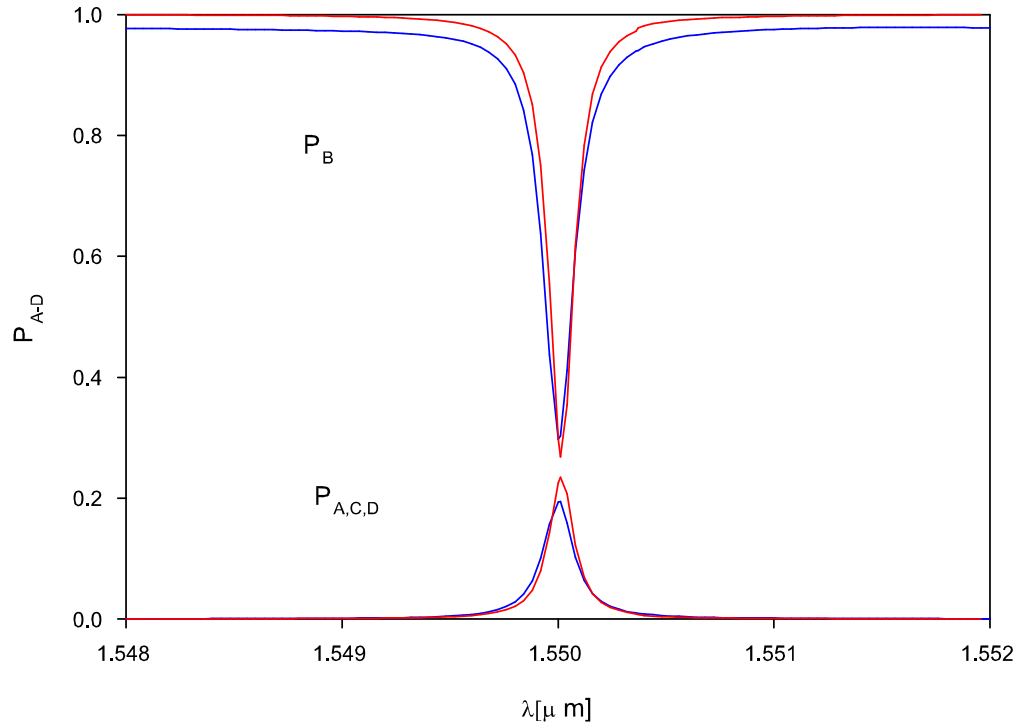
In order to estimate numerically the accuracy of the present simulation in terms of the resonant wavelengths we compare the CMT result with those of rigorous numerical computations *Olympios*. As a measure of accuracy of the present result, we use the error rate defined by

$$(\text{error rate}) \equiv \frac{|\lambda_r^{(n)} - \lambda_O^{(n)}|}{\lambda_O^{(n)}} \quad (3.2)$$

for $n = 1, 2, 3, 4$ and 5 , where λ_r and λ_O denotes resonant wavelengths of CMT and *Olympios*, respectively. Table 3.3 shows the error rates of the resonant wavelengths. It is observed that our results are good in agreement with the *Olympios* ones.

n	<i>Olympios</i> (μm)	CMT (μm)	error rate
1	1.535470	1.535490	1.302×10^{-5}
2	1.542280	1.542320	2.594×10^{-5}
3	1.550000	1.550010	6.452×10^{-6}
4	1.557720	1.55783	7.062×10^{-5}
5	1.565130	1.56522	5.750×10^{-5}

Table 3.3: Resonant wavelengths and error rates

Figure 3.8: The spectral resonance of CMT plotted with red lines and *Olympios* with blue lines around $\lambda_0 = 1.55 \mu\text{m}$.

In Fig. (3.6) up to $\lambda \approx 1.58 \mu\text{m}$ we can see that the trend of the shape of the CMT simulation coincides well with *Olympios*. However, as we can see in Fig. (3.11) in the wavelength range $1.58 < \lambda < 1.6 \mu\text{m}$, other minors resonances appear, which are not shown by the CMT results.

Furthermore the CMT shows spectral distance between two neighboring resonance $\Delta\lambda$ of about 7.6 nm. The same value of $\Delta\lambda$ is also more less given by *Olympios*. Nevertheless, from Table 3.6 and by considering the spectrum around one of the resonance wavelengths (i.e $\lambda_r^3 = 1.55 \mu\text{m}$) we can see that apparently the spectral resonance curve of CMT is little bit shifted to the right with the spectral curve of *Olympios* as a reference. By calculating the FSR $\Delta\lambda$, where it is defined by

$$\Delta\lambda_k = \left| \lambda^{(k+1)} - \lambda^{(k)} \right|, \text{ for } k = 1, \dots, 4 \quad (3.3)$$

we know that all points of the curve are shifted to the right. Table 3.4 shows the FSR of CMT and BEP simulations.

Apart from that if we look to the relative power calculated at the ports in Fig. (3.6), apparently the power at port B P_B predicted by CMT is in general higher than P_B predicted by *Olympios*. It is remarkable because the CMT is constructed under the assumption that no radiation mode is included and the interaction between the port waveguides and the grating is neglected. Consequently, the power indeed can be transferred without losses that usually comes from the radiation.

	$\Delta\lambda_1$	$\Delta\lambda_2$	$\Delta\lambda_3$	$\Delta\lambda_4$
<i>Olympios</i>	6.80	7.72	7.72	7.41
CMT	6.83	7.69	7.82	7.39

Table 3.4: Free Spectral Range $\Delta\lambda$ of CMT and BEP simulation

In order to explain the deviation of the resonance position of CMT simulation from the *Olympios* results, let us consider Eq.(2.65). This equation can be rewritten to be

$$\lambda_0 = \frac{L(2\pi\tilde{N}_{\text{eff}})}{(l\pi + \varphi)} \quad (3.4)$$

According to Eq. (3.4) λ_0 is determined by four parameters: \tilde{N}_{eff} , φ , L , and l . Since l and L are known beforehand, and \tilde{N}_{eff} is the effective index of 5th order mode of the cavity waveguide and it is known accurately, therefore the precise λ_0 is determined only by φ given by the complex valued amplitude reflection coefficient r . Substituting l , L , \tilde{N}_{eff} into Eq. (3.4) and the CMT results for $\lambda_r^3 = 1.550010 \mu\text{m}$, corresponds to $\varphi = -0.0720771$ and the *Olympios* result $\lambda_O^3 = 1.55 \mu\text{m}$ to $\varphi = -0.065288$. Taken *Olympios* as a reference, the spectral resonance is shifted because of a error in φ or r of the CMT simulation for the grating. Note that for the reflectance R , the CMT gives accurate results when compared to *Olympios* (see Fig. 3.9).

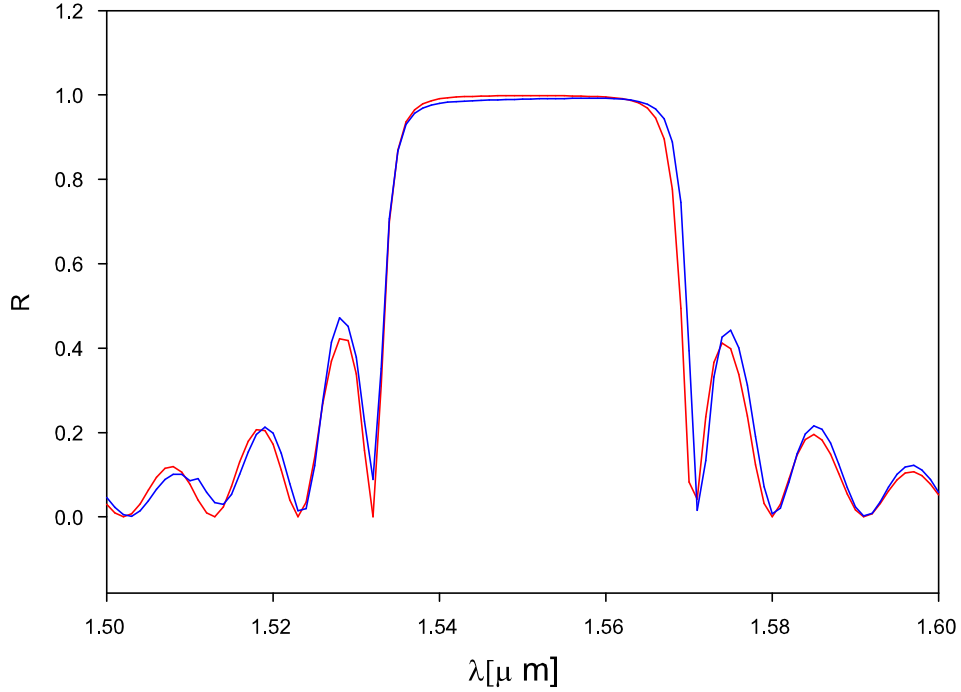


Figure 3.9: Reflectance curve of the Bragg-gratings. The red curve corresponds to CMT simulations, the blue curve to *Olympios*.

3.2.2 Nonsymmetric Bragg-reflectors

As we can see from previous results the resonances are present within the stopband region and we know that the region (i.e bandwidth) is only determined by the grating of the Bragg-reflectors. It means the peaks are restricted to the wavelength interval that is defined by the high reflectivity region of the Bragg reflectors. Thus this property enables us to modify the spectral characteristic of the resonances, for instance the number of resonant wavelengths, by only changing the grating parameters.

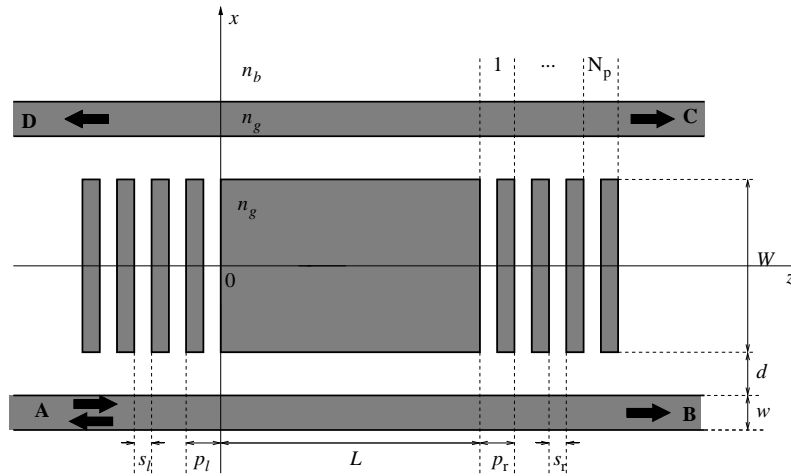


Figure 3.10: Nonsymmetric grating assisted rectangular microresonator.

Theoretically the left and right grating can be designed such that it gives characteristics such as a broad or narrow stopband (bandwidth) or such that it shows other properties, for instance a shift in the curve of reflectance R . However the bandwidth of the Bragg-reflectors is determined by the fractional difference of the index of refraction of the neighboring layers [18] and the index is kept fix in this simulation. Thus instead of changing the index of refraction of the grating we can tune the geometrical parameters s and p .

What we would like to aim at in this section is a device that shows a single resonant wavelength which is realised with nonsymmetrical detuned Bragg-reflectors. In the previous simulation we put identical Bragg-reflectors at the left and the right cavity facets. For the sake of a single resonance in this simulation we let them be different. Let us then introduce two pairs of

the grating parameters: (p_r, s_r) denotes the grating parameters of the right grating and (p_l, s_l) for the left grating (see Fig. 3.10). What we are going to do is that first we keep $s_r = s_l = s$ constant and tune p_l and p_r , second it is the other way around, keep $p_l = p_r = p$ and vary s . The values of p and s are given in Table (3.2). The simulation results are shown in Fig. (3.11) and Fig. (3.12).

For the first simulation, Fig. (3.11), we select $p_r = 1.549 \mu\text{m}$ and $p_l = 1.523 \mu\text{m}$ for the grating parameters which refers to the values given in [8]. Along with the period length the complex reflection coefficients of the gratings at the target wavelength λ_0 change. Therefore, the cavity length should be slightly adjusted to a new values $L = 80.006 \mu\text{m}$ in order to reestablish the resonance at λ_0 . [9]

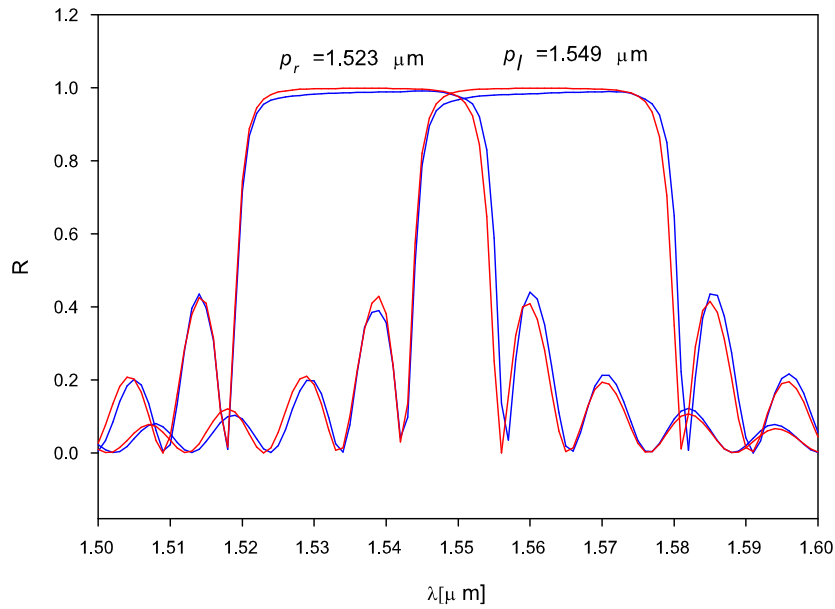
Fig. (3.11a) shows the spectral reflectance of the left and right Bragg-reflectors of the solution of CMT for the structure shown in Fig. (3.4). In this figure it can be seen that the reflectance R of the left and right gratings overlaps with $\lambda_0 = 1.55 \mu\text{m}$ as a center, where the width of the overlap is about $0.015 \mu\text{m}$. This width covers the wavelength range from $1.543 \mu\text{m}$ to $1.558 \mu\text{m}$. The overlap becomes the actual spectral reflectance due to non-symmetric reflectors. As expected, it implies the spectral resonance shown in Fig. (3.11) in which there is only one pronounced resonant wavelength. From this figure, it can be seen that CMT is in a good agreement with *Olympios*.

In the second simulation we select $s_r = 0.181 \mu\text{m}$ and $s_l = 0.381 \mu\text{m}$ and we keep p constant. These parameters are obtained by numerical experiments of the grating using the CME given in Eq. (2.53). In this simulation we take L of $79.985 \mu\text{m}$. As we can see in Fig. (3.12), with this setting CMT gives more less the same result as before in which p is adjusted. This is verified by *Olympios* which shows more less the same resonance curve.

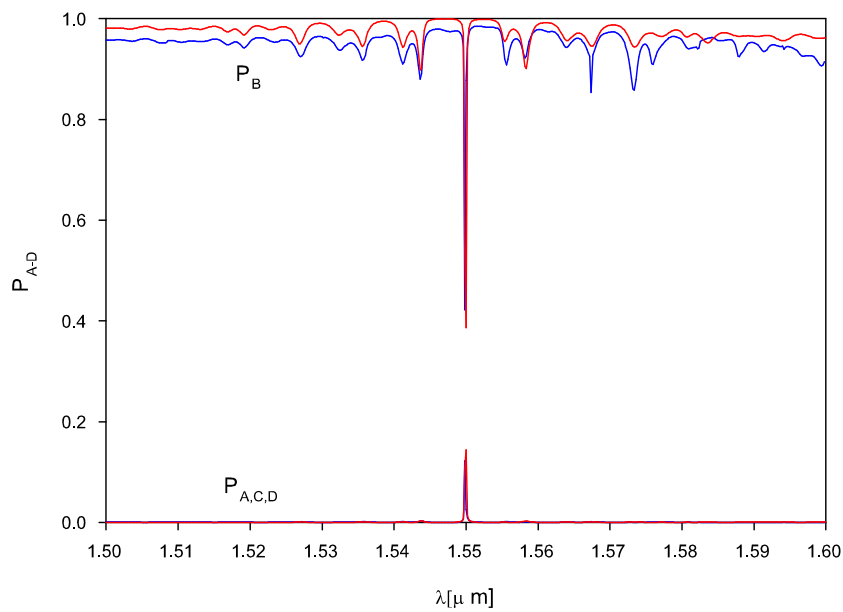
With respect to the present problems, apparently CMT simulation results are quite adequate when compared to *Olympios* ones.

3.2.3 Filter simulations

While at resonance the present device distributes the input among all four ports, a filter that properly drops the power into a single port can be realised

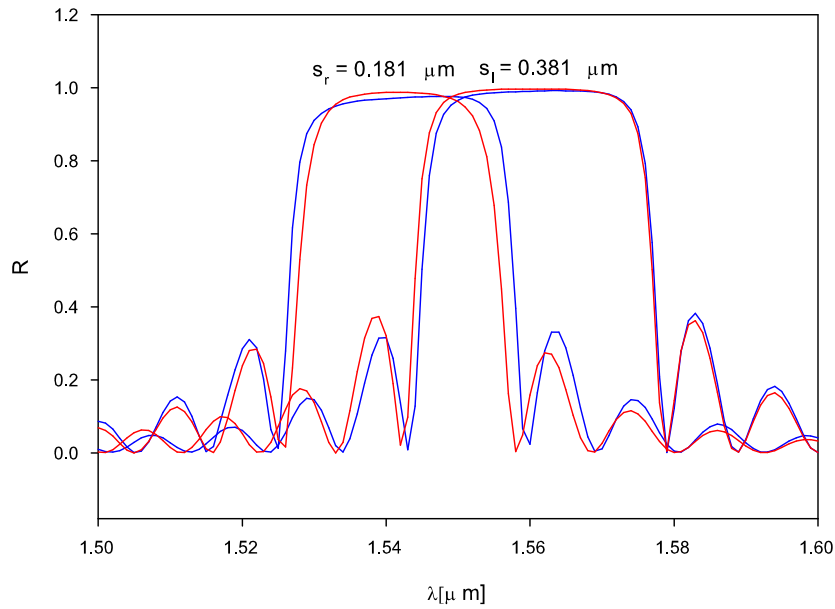


(a)

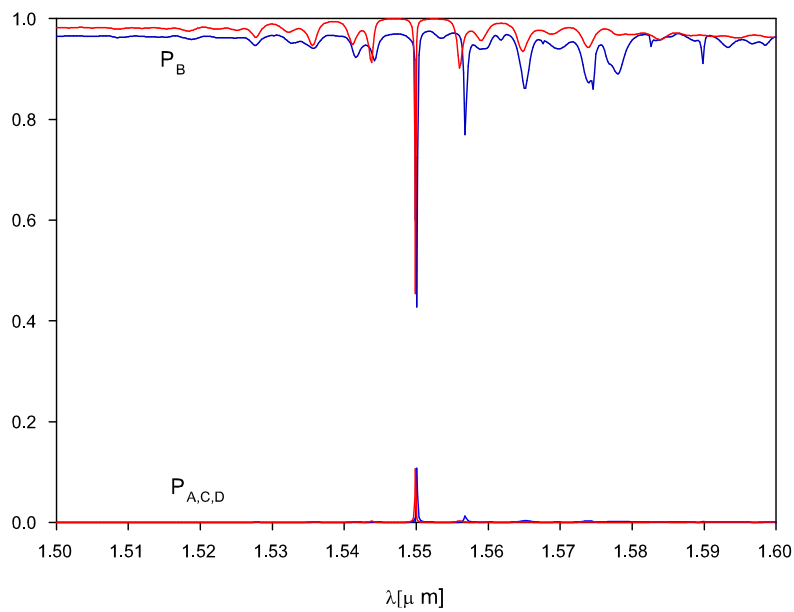


(b)

Figure 3.11: (a) Spectral reflectance of Bragg-reflectors, red curve from CMT while blue curve from *Olympios*. (b) Spectral resonance of Nonsymmetrical grating assisted resonators with $p_l = 1.538 \mu\text{m}$ and $p_r = 1.549 \mu\text{m}$, red lines correspond to CMT simulation, blue lines to *Olympios*.



(a)



(b)

Figure 3.12: (a) Spectral reflectance of Bragg-reflectors. The red curve represents the results from the approximative CMT, while the blue curve corresponds to the *Olympios*. (b) Spectral resonance of Nonsymmetrical grating assisted resonators with $s_l = 3.81 \mu\text{m}$ and $s_r = 1.81 \mu\text{m}$, red lines correspond to CMT simulation, blue lines to *Olympios*.

with two cascaded single cavity resonators. The idea is firstly introduced in papers for the case without the gratings [14, 12]. The configuration of the device can be seen in Fig. (3.13). The simulation in this section employs the number of periods N_m of the middle grating provided in [8] with $N_m = 33$; the others parameters remain. Compared to the single cavity configuration one new parameter introduced in this configuration is the distance between the individual cavities. Thus two cavities are spaced by a distance g given by $N_m p + s = 51.035 \mu\text{m}$. Due to the presence of this shorter grating, we can expect that there is a direct interaction between the separated cavities to establish the desired type of resonance.

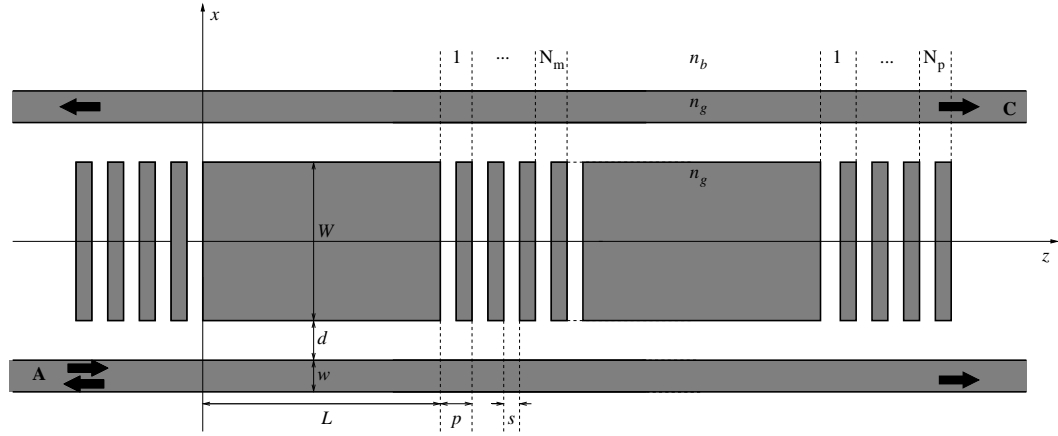


Figure 3.13: Schematic of an add-drop filter based on two cascaded identical rectangular microresonators. Compared to Fig. (2.1), in between the cavities a grating is present with the number of periods N_m introduced as an additional parameter.

For this device, we use the same treatment as when deriving CMT for a single cavity in which the coupling between the ports and the grating is neglected. Consequently, the mode amplitude of forward and backward propagating fields of the ports at $z = L + g$ can be defined by

$$\begin{aligned} \mathbf{F}_p(L + g) &= \mathbf{F}_p(L) \exp(-j\beta g), \\ \mathbf{B}_p(L) &= \mathbf{B}_p(L + g) \exp(j\beta g), \end{aligned} \quad (3.5)$$

respectively. Let us consider again the solution of CME given in section 1

of the previous chapter, Eq. (2.18) and Eq. (2.20). Using this solution, the amplitude of the forward propagating fields at $z = 2L + g$ is given by

$$\mathbf{F}(2L + g) = \mathbf{T}(L)\mathbf{F}(L + g), \quad (3.6)$$

and the backward ones at $z = L + g$

$$\mathbf{B}(L + g) = \mathbf{T}(L)\mathbf{B}(2L + g), \quad (3.7)$$

respectively; notice that no incoming field is launched at the right $\mathbf{B}_p(2L + g) \equiv 0$. Due to the presence of the grating $F_c(L + g)$ and $B_c(L)$ are defined as follows:

$$F_c(L + g) = t_m F_c(L) + r_m B_c(L + g) \quad (3.8)$$

and

$$B_c(L) = t_m B_c(L + g) + r_m F_c(L). \quad (3.9)$$

Parameters r_m and t_m appearing in Eqs. (3.8) and (3.9) are reflection and transmission coefficients of the middle grating given by Eq. (2.53).

Combining Eqs. (2.18), (2.20), (3.5) to (3.9), we obtain

$$\begin{aligned} \mathbf{F}_p(2L + g) &= T_{pp} \exp(-j\beta g) \mathbf{F}_p(L) + T_{pc} r_m T_{cc} F_c(2L + g) \\ \mathbf{B}_p(0) &= (T_{pp} T_{pc} r \exp(j\beta g) + T_{pct} t_m T_{cc} r) F_c(2L + g) + T_{pc} r_m F_c(L) \end{aligned} \quad (3.10)$$

for the transmission through the device and for the reflection caused by the resonator, while the field inside the cavity given by

$$F_c(2L + g) = \Omega^{-1} [(T_{cp} \exp(-j\beta g) \mathbf{F}_p(L) + T_{cct} t_m F_c(L)] \quad (3.11)$$

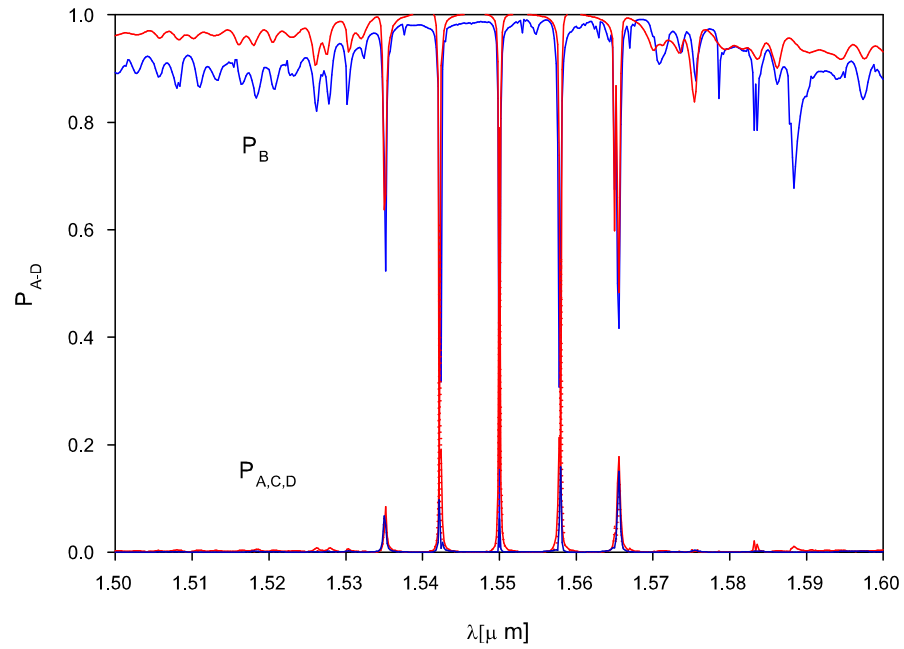
with $\Omega = 1 - T_{\text{cc}r\text{m}r}^2$. The forward propagating fields at $z = L$ $\mathbf{F}(L)$ are given by Eq. (2.57) with $B_{\text{C}}(0)$ defined as follows:

$$B_{\text{C}}(0) = \{1 - [\Omega^{-1}(T_{\text{cp}}T_{\text{pc}r} \exp(j\beta g) + T_{\text{cc}t\text{m}r}^2)(T_{\text{cc}t\text{m}r}^2 + T_{\text{cp}}T_{\text{pc}r} \exp(-j\beta g) + T_{\text{cc}r\text{m}})]\}^{-1} \{[\Omega^{-1}(T_{\text{cp}}T_{\text{pc}r} \exp(j\beta g) + T_{\text{cc}t\text{m}r}^2)(T_{\text{cc}t\text{m}r}^2)(T_{\text{cc}t\text{m}T_{\text{cp}}} + T_{\text{cp}}T_{\text{pc}r} \exp(-j\beta g)T_{\text{pp}}) + T_{\text{cc}r}\} \mathbf{F}_{\text{P}}(0) \quad (3.12)$$

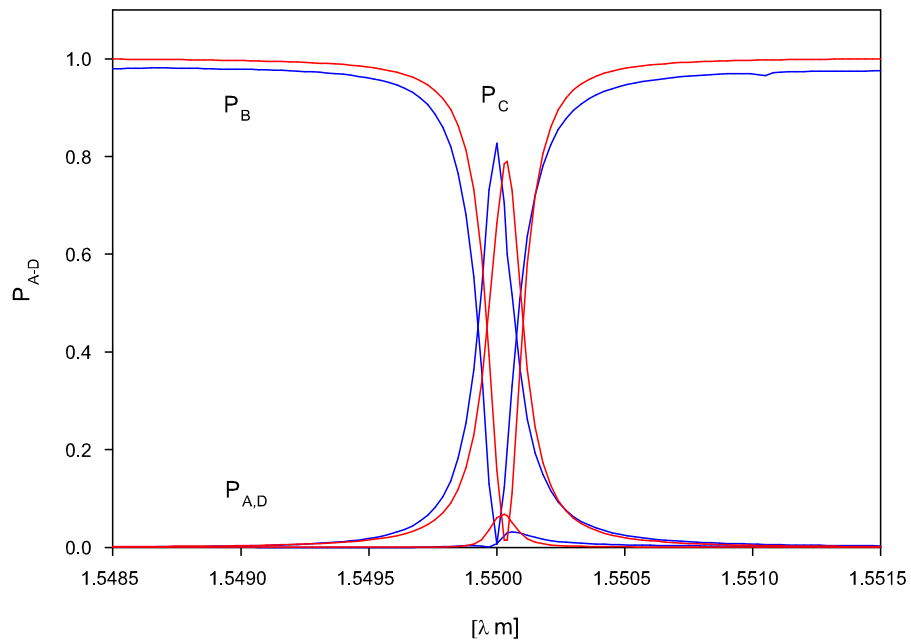
The simulation results of CMT and *Olympios* for this configuration are shown in Fig. (3.14). From this result we can see that the trend of spectral response obtained CMT simulation is in good agreement to the *Olympios* results. CMT predicts that the extremal transfer is reached at $\lambda_r = 1.55003 \mu\text{m}$ in which a major part of the power is dropped in the forward direction into port C, while about 1% of the input power is reflected to ports A and C or transmitted to B. *Olympios* locates the resonance precisely at $\lambda_{\text{O}} = 1.55 \mu\text{m}$.

Using Eq. (3.2), we can calculate that the error of the CMT calculation compared to *Olympios* is about 1.953×10^{-5} when looking at the highest peak in port C. Compared to the previous calculation for single cavity, the error obtained in this calculation is quite similar.

The corresponding field pattern in Fig. (3.15) shows simultaneously appearing high intensities in both cavities.



(a)



(b)

Figure 3.14: Spectral resonance of a filter device according to CMT (solid red line) and *Olympios* plotted (solid blue line). (b) Extremal relative levels of power transmission are predicted at the resonance wavelength

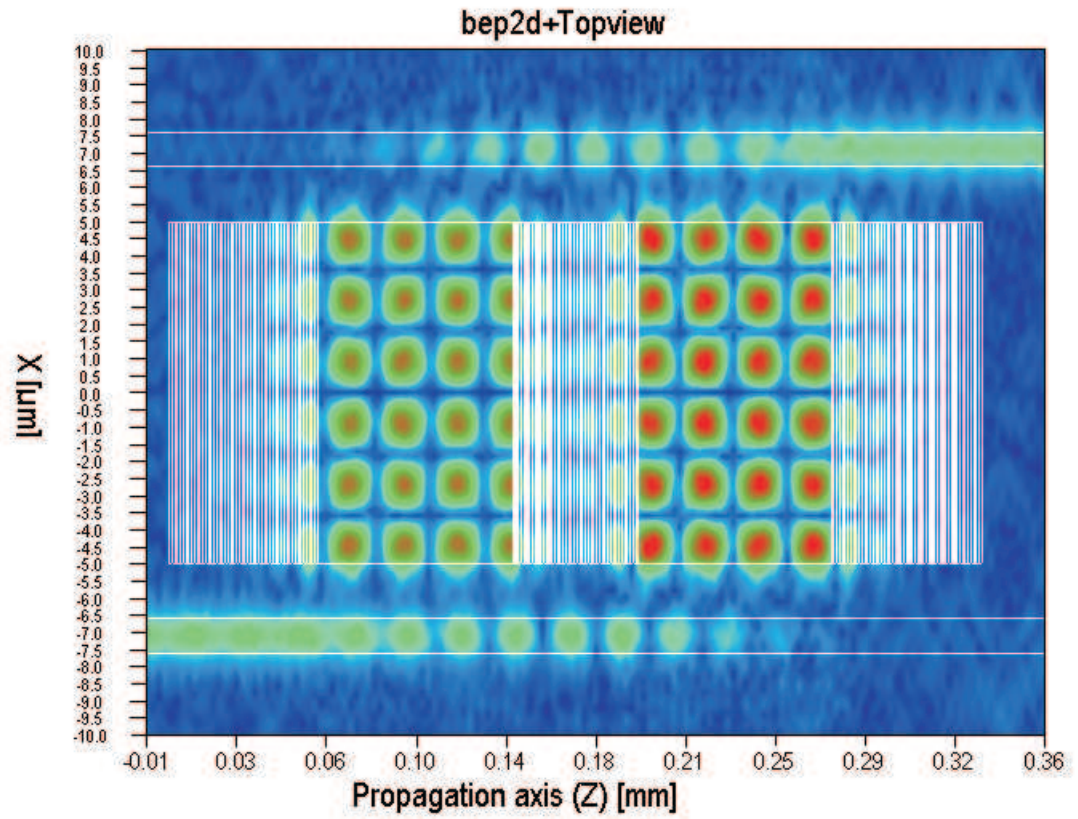


Figure 3.15: Field pattern at resonance $|\mathcal{E}|^2$, for a grating assisted rectangular microresonator with two cavities for $\lambda_0 = 1.55 \mu\text{m}$.

Chapter 4

Conclusions and remarks

In conclusion, coupled mode theory can be successfully applied to the analysis of the grating assisted rectangular microresonator structure. We have presented the derivation of a coupled-mode formulation and given its general solution for the resonator device. The general solution is obtained by splitting the problem into two: the cavity segment and the Bragg-reflectors. Furthermore the parts are investigated separately under the assumption that the coupling between the port waveguides and the grating can be neglected and that the interaction between the confined modes of the port waveguides and one specific guided mode of the cavity is relevant. For the simulations of the Bragg-reflectors we have employed contradirectional coupled-mode theory, based on the forward and backward traveling versions of a corresponding guided mode supported by the cavity core.

We have analysed the process of determining suitable parameters for the device with the aid of the CMT formulation. Based on the solution of CME and the parameters, we have presented some simulation results of CMT simulations for several configurations: symmetrical and non symmetrical resonators and a filter device. For the sake of comparison we also presented results of rigorous numerical computations (BEP, *Olympios*).

From the results, we have found good agreement between the approximate CMT model and *Olympios*. Concerning the position of resonances the error of the CMT results compared to the more accurate BEP is in the order of 10^{-5} . Since no radiation is included and some (crude) approximations

are made (e.g. the interaction between the port waveguides and the Bragg grating neglected) in the CME derivation, it leads no perfect coincidence can be expected. Nevertheless, the numerical simulations have verified our theoretical predictions, hence we can conclude that our CMT model is quite adequate to describe the presented problems.

The calculations with CMT are much efficient. For illustration, the length of time required by CMT to perform the computations to get the results shown in Fig. (3.11) is only a few minutes, while *Olympios* takes about almost a day. Apart from that, the *Olympios* computations require much more computer memory and hard disk space to store the simulation results.

Appendix A

Cholesky Decomposition

A symmetric and positive definite matrix can be efficiently decomposed into a lower and upper triangular matrix. Using LU decomposition we can factorise $A = LU$. If A satisfies the above criteria, we can decompose more efficiently into $A = CC^T$, where C is a lower triangular matrix with positive diagonal elements. To solve $Ax = b$, we solve firstly $Cy = b$ for y , and then $C^T x = y$ for x .

To derive $A = CC^T$, we simply equate coefficients on both sides of the equation:

$$\begin{bmatrix} a_{11} & a_{12} & \dots & a_{1n} \\ a_{21} & a_{22} & \dots & a_{2n} \\ \vdots & \vdots & \ddots & \vdots \\ a_{n1} & a_{n2} & \dots & a_{nn} \end{bmatrix} = \begin{bmatrix} c_{11} & 0 & \dots & 0 \\ c_{21} & c_{22} & \dots & 0 \\ \vdots & \vdots & \ddots & 0 \\ c_{n1} & c_{n2} & \dots & c_{nn} \end{bmatrix} \begin{bmatrix} c_{11} & c_{21} & \dots & c_{n1} \\ 0 & c_{22} & \dots & c_{n2} \\ \vdots & \vdots & \ddots & \vdots \\ 0 & 0 & \dots & c_{nn} \end{bmatrix}$$

to obtain in general for $i = 1, \dots, n$ and $j = i + 1, \dots, n$:

$$c_{ii} = \sqrt{\left(a_{ii} - \sum_{k=1}^{i-1} c_{ik}^2 \right)},$$
$$c_{ji} = \left(a_{ji} - \sum_{k=1}^{i-1} c_{jk} c_{ik} \right) / c_{ii}$$

Since A is symmetric and positive definite, the expression under the square root is always positive, and all c_{ij} are real.

Appendix B

Matlab Code

MATLAB programs implementing of the CMT have been written to simulate the grating assisted rectangular microresonator devices. A listing of the code is the following.

Main program

```
clear

nl = 1.6; %refractive index of guided system

nr = 1.45; %refractive index of background

PA = []; PB = []; PC = []; PD = []; l=[];

for lmd = 1.5:0.00001:1.6; %vacuum wavelength

l = [l,lmd];

k = 2*pi/lmd; %wave number

m0 = 4*pi*10^-13; %permeability in vacuum

e0 = 8.854*10^-18; %permittivity in vacuum

omg =k*3*10^14; %harmonic frequency

Fp0 = [1 0]'; % Incoming field

M = zeros(3,3); K = zeros(3,3);

%information about rectangular part
```

```

W = 9.955; %the width of cavity

S = W/2; % half of cavity's width

w = 1; % the width of port

d = 1.6; % length of gap between cavity and port waveguide

Z = 79.985; % Length of cavity

%Z = 79.985; %information about assisted Bragg grating

Pr = 1.538; %Length of periode of grating

Pl = 1.538; N = 40; %Number of periode

L = N*Pr; %Length of the grating

sr = 0.281; %the distance between two high refractive index right grating sl

= 0.281; %the distance between two high refractive index left grating

dn = nr-nl; %index contrast

ndelta = nl^2-nr^2;

MM = 1; %mode number which is being taken inside the port

NN = 6; %mode number for cavity

NeffP = modesolv(nl,nr,lmd,w,MM); %effective index of port

NeffC = modesolv(nl,nr,lmd,W,NN); %effective index of cavity

betaP = k*NeffP;

betaC = k*NeffC;

kx1P = k*sqrt(NeffP^2-nr^2); % propagation in x in background of port

kx1C = k*sqrt(NeffC^2-nr^2); % propagation in x in background of cavity

kx2P = k*sqrt(nl^2-NeffP^2); % propagation in x in ports

kx2C = k*sqrt(nl^2-NeffC^2); % propagation in x in cavity

%Normalised Amplitude

A2=sqrt((2*omg*m0/betaP)*(exp(kx1P*d)/(2*kx1P)*((cos(kx2P*w/2)+kx2P*sin(kx2P*w/2))/((1+kx1P)*exp(kx1P*d/2)))^2+(sin(kx2P*w)/(2*kx2P)+(2*kx1P)^-1*((cos(kx2P*w/2)-kx2P*sin(kx2P*w/2))/(1-kx1P))^2)^-1);

```

```

A8=sqrt((2*omg*m0/betaC)*(exp(kx1C*d)/(2*kx1C)*((-sin(kx2C*S)+kx2C*cos(kx2C*S))/((1+kx1C)*exp(kx1C*d/2)))^2+(-
sin(2*kx2C*S)+2*kx2C*S)/(2*kx2C)+(exp(kx1C*d)/(2*kx1C))*((sin(kx2C*S)+kx2C*cos(kx2C*S))/((1-
kx1C)*exp(kx1C*d/2)))^2)^-1);

A11=sqrt((2*omg*m0/betaP)*(1/(2*kx1P)*((cos(kx2P*w/2)+kx2P*sin(kx2P*w/2))/(1+kx1P))^2+
(sin(kx2P*w)+kx2P*w)/(2*kx2P)+(exp(kx1P*d)/(2*kx1P))*((cos(kx2P*w/2)-
kx2P*sin(kx2P*w/2))/((1-kx1P)*exp(kx1P*d/2)))^2)^-1);

A1=((cos(kx2P*w/2)-kx2P*sin(kx2P*w/2))/(1-kx1P))*A2;

A5=((cos(kx2P*w/2)+kx2P*sin(kx2P*w/2))/((1+kx1P)*exp(kx1P*d/2)))^2*A2;

A4 = ((sin(kx2C*S)+kx2C*cos(kx2C*S))/((1-kx1C)*exp(kx1C*d/2)))^2*A8;

A9 = ((-sin(kx2C*S)+kx2C*cos(kx2C*S))/((1+kx1C)*exp(kx1C*d/2)))^2*A8;

A10 = ((cos(kx2P*w/2)-kx2P*sin(kx2P*w/2))/((1-kx1P)*exp(kx1P*d/2)))^2*A11;

A13 = ((cos(kx2P*w/2)+kx2P*sin(kx2P*w/2))/(1+kx1P))^2*A11;

%A = [A1 A2 A4 A5 A8 A9 A10 A11 A13]; %the mode amplitude of sparated parts

%Element of matrix M (power coefficient)

M(2,2)=(betaP/(2*omg*m0))*(exp(kx1P*d)*A5^2/(2*kx1P)+(sin(kx2P*w)+kx2P*w)*
A2^2/(2*kx2P)+A1^2/(2*kx1P));

M(3,3)=(betaC/(2*omg*m0))*(exp(kx1C*d)*A9^2/(2*kx1C)+(-sin(2*kx2C*S)+
2*kx2C*S)*A8^2/(2*kx2C)+exp(kx1C*d)*A4^2/(2*kx1C));

M(1,1)=(betaP/(2*omg*m0))*(A13^2/(2*kx1P)+(sin(kx2P*w)+kx2P*w)*A11^2/(2*kx2P)+exp(kx1P*d)*A10^2/(2*kx1P));

M(1,2)=(betaP/(2*omg*m0))*(A13*A5*exp(-0.5*kx1P*(4*S+3*d+2*w))/(2*kx1P)+A11*A5*(kx1P*cos(0.5*kx2P*w)+
kx2P*sin(0.5*kx2P*w))*exp(-0.5*kx1P*(4*S+3*d))/(kx1P^2+kx2P^2)+A11*A5*(-kx1P*cos(0.5*kx2P*w)+kx2P*
sin(0.5*kx2P*w))*exp(-0.5*kx1P*(4*S+3*d+2*w))/(kx1P^2+kx2P^2)+2*A10*A5*(S+d)*exp(-kx1P*(2*S+d))+
A10*A2*(-kx1P*cos(0.5*kx2P*w)+kx2P*sin(0.5*kx2P*w))*exp(-0.5*kx1P*(4*S+3*d+2*w))/(kx1P^2+kx2P^2)+
A10*A2*(kx1P*cos(0.5*kx2P*w)+kx2P*sin(0.5*kx2P*w))*exp(-0.5*kx1P*(4*S+3*d))/(kx1P^2+kx2P^2)+A10*
A1*exp(-0.5*kx1P*(4*S+3*d+2*w))/(2*kx1P);

M(2,1)=M(1,2);

if

```



```

kx1P==kx1C M(1,3)=(1/(4*omg*m0))*(betaP+betaC)*(A13*A9*exp(-0.5*kx1C*(d+2*w))/(kx1P+kx1C)+A11*A9*(-
exp(-1/2*kx1C*
d-kx1C*w)*kx1C*cos(1/2*kx2P*w)+exp(-1/2*kx1C*d-kx1C*w)*kx2P*sin(1/2*kx2P*w)+exp(-1/2*kx1C*d)*kx1C*
cos(1/2*kx2P*w)+exp(-1/2*kx1C*d)*kx2P*sin(1/2*kx2P*w))/(kx1C^2+kx2P^2)+A10*A9*d+(-kx2C*cos(kx2C*S)-
kx1P*sin(kx2C*S))*exp(-0.5*kx1P*(4*S+d))*A8*A10/(kx1P^2+kx2C^2)+(kx2C*cos(kx2C*S)-kx1P*sin(kx2C*S))*
exp(-0.5*kx1P*d)*A8*A10/(kx1P^2+kx2C^2)+A10*A4*exp(-2*kx1P*S-1/2*kx1P*d+1/2*kx1C*d)/(kx1P+kx1C));
M(3,2)=-M(1,3);
else
M(1,3)=(1/(4*omg*m0))*(betaP+betaC)*(A13*A9*exp(-0.5*kx1C*(d+2*w))/(kx1P+kx1C)+A11*A9*(-
exp(-1/2*kx1C*
d-kx1C*w)*kx1C*cos(1/2*kx2P*w)+exp(-1/2*kx1C*d-kx1C*w)*kx2P*sin(1/2*kx2P*w)+exp(-1/2*kx1C*d)*
kx1C*cos(1/2*kx2P*w)+exp(-1/2*kx1C*d)*kx2P*sin(1/2*kx2P*w))/(kx1C^2+kx2P^2)+A10*A9*(exp(-
1/2*kx1P*
d+1/2*kx1C*d)-exp(1/2*kx1P*d-1/2*kx1C*d))/(-kx1P+kx1C)+(-kx2C*cos(kx2C*S)-kx1P*sin(kx2C*S))*exp(-
0.5*
kx1P*(4*S+d))*A8*A10/(kx1P^2+kx2C^2)+(kx2C*cos(kx2C*S)-kx1P*sin(kx2C*S))*exp(-0.5*kx1P*d)*A8*
A10/(kx1P^2+kx2C^2)+A10*A4*exp(-2*kx1P*S-1/2*kx1P*d+1/2*kx1C*d)/(kx1P+kx1C));
M(3,2) = -M(1,3);
end
M(3,1)=M(1,3); M(2,3)=M(3,2);
%Element of matrix K (coupling coefficient)
K(1,3)=ndelta*(e0*omg/8)*(A11*A9*(-exp(-1/2*kx1C*d-kx1C*w)*kx1C*cos(1/2*kx2P*w)+exp(-1/2*kx1C*d-
kx1C*w)*kx2P*sin(1/2*kx2P*w)+exp(-1/2*kx1C*d)*kx1C*cos(1/2*kx2P*w)+exp(-1/2*kx1C*d)*kx2P*sin(1/2*
kx2P*w))/(kx1C^2+kx2P^2)-A8*A10*(exp(-2*kx1P*S-1/2*kx1P*d)*kx2C*cos(kx2C*S)+exp(-2*kx1P*S-
1/2*
kx1P*d)*kx1P*sin(kx2C*S)-exp(-1/2*kx1P*d)*kx2C*cos(kx2C*S)+exp(-1/2*kx1P*d)*kx1P*sin(kx2C*S))/

```

```

(kx1P^2+kx2C^2)+2*A10*A4*(-exp(-2*kx1P*S-3/2*kx1P*d-kx1P*w-1/2*kx1C*d-kx1C*w)+exp(-
2*kx1P*S-3/2*
kx1P*d-1/2*kx1C*d))/(kx1P+kx1C);
K(3,1)=K(1,3);
K(3,2)=ndelta*(e0*omg/8)*(2*A5*A9*(-exp(-2*kx1P*S-3/2*kx1P*d-kx1P*w-1/2*kx1C*d-kx1C*w)+exp(-
2*kx1P*
S-3/2*kx1P*d-1/2*kx1C*d))/(kx1P+kx1C)+A8*A5*(exp(-2*kx1P*S-1/2*kx1P*d)*kx2C*cos(kx2C*S)+exp(-
2*
kx1P*S-1/2*kx1P*d)*kx1P*sin(kx2C*S)-exp(-1/2*kx1P*d)*kx2C*cos(kx2C*S)+exp(-1/2*kx1P*d)*kx1P*s
in(kx2C*S))/(kx1P^2+kx2C^2)+A2*A4*(-kx1C*cos(0.5*kx2P*w)+kx2P*sin(0.5*kx2P*w))/(kx1C^2+kx2P^2)*
exp(-0.5*kx1C*(d+2*w))+A2*A4*(kx1C*cos(0.5*kx2P*w)+kx2P*sin(0.5*kx2P*w))/(kx1C^2+kx2P^2)*exp(-
0.5*d*kx1C);
K(2,3)=K(3,2);
K(1,2)=ndelta*(e0*omg/8)*(A11*A5*(exp(-2*kx1P*S-3/2*kx1P*d)*kx1P*cos(1/2*kx2P*w)+exp(-
2*kx1P*S-3/2*
kx1P*d)*kx2P*sin(1/2*kx2P*w)-exp(-2*kx1P*S-3/2*kx1P*d-kx1P*w)*kx1P*cos(1/2*kx2P*w)+exp(-
2*kx1P*S-
3/2*kx1P*d-kx1P*w)*kx2P*sin(1/2*kx2P*w))/(kx1P^2+kx2P^2)+4*S*A5*A10*exp(-kx1P*(2*S+d))+A2*A10*
(exp(-2*kx1P*S-3/2*kx1P*d)*kx1P*cos(1/2*kx2P*w)+exp(-2*kx1P*S-3/2*kx1P*d)*kx2P*sin(1/2*kx2P*w)-
exp(-2*kx1P*S-3/2*kx1P*d-kx1P*w)*kx1P*cos(1/2*kx2P*w)+exp(-2*kx1P*S-3/2*kx1P*d-kx1P*w)*kx2P*
sin(1/2*kx2P*w))/(kx1P^2+kx2P^2);
K(2,1) = K(1,2);
K(2,2)=ndelta*(e0*omg/8)*A5^2*(exp(-kx1P*(4*S+3*d))+exp(-d*kx1P)-exp(-kx1P*(4*S+3*d+2*w))-
exp(-kx1P*(4*S+d)))/kx1P;K(3,3)=ndelta*(e0*omg/8)*(A4^2*(-exp(-1/2*kx1C*(d+2*w))^2+exp(-
1/2*kx1C*
d)^2)/kx1C+A9^2*(-exp(-1/2*kx1C*(d+2*w))^2+exp(-1/2*kx1C*d)^2)/kx1C);
K(1,1)=ndelta*(e0*omg/8)*(-A10^2*(exp(-1/2*kx1P*(4*S+d))^2-exp(-1/2*kx1P*d)^2)/kx1P+-A10^2*

```

```

(exp(-1/2*kx1P*(4*S+3*d+2*w))^2-exp(-1/2*kx1P*(4*S+3*d))^2)/kx1P);

beta = (betaP+betaC)*0.5;

H = beta*M+K; O = chol(M); % cholesky decomposition

HH = inv(O)'*H*inv(O);

[WW,bsuper] = eig(HH);

bsuper = diag(bsuper); % supermode

for j = 1 : length(bsuper)

    a(:,j) = inv(O)*WW(:,j);

end

dumm = 0;

for ii =1:length(bsuper)

    dumm = dumm + (exp(-i*bsuper(ii)*Z)*a(:,ii)*(a(:,ii))');

end

T = O*dumm*O'; %Propagation matrix

% Split matrix

Tcc = T(3,3);

Tpp = [ T(1,1) T(1,2) T(2,1) T(2,2)];

Tpc = [ T(1,3) T(2,3)];

Tcp = [ T(3,1) T(3,2)];

Rr = gratpartm(nl,nr,W,Pr,N,sr,lmd,NeffC,NN,1); % coefficient of reflectivity of righth grating

Rl = gratpartm(nl,nr,W,Pl,N,sl,lmd,NeffC,NN,1); % coefficient of reflectivity of left grating %R =
1; Omega = 1 - Tcc*Rr*Tcc*Rl;

FpL = (Tpp + Tpc*Rl*inv(Omega)*Tcc*Rr*Tcp)*Fp0;

FcL = (Tcp+Tcc*Rl*inv(Omega)*Tcc*Rr*Tcp)*Fp0;

Bp0 = Tpc*Rr*FcL; Bc0 = inv(Omega)*Tcc*Rr*Tcp*Fp0;

PA = [PA, abs(Bp0(1,:))^2];

PB = [PB, abs(FpL(1,:))^2];

```

```
PC = [PC, abs(FpL(2,:))^2];
```

```
PD = [PD, abs(Bp0(2,:))^2];
```

```
end
```

Grating part

```
function y = gratpart(n1,n2,Width,Periode, NPeriode, space, lambda,neff,MNum,Pil)
```

```
R = []; RR=[]; T = []; Pz = [];
```

```
L = NPeriode*Periode;
```

```
dn = n2-n1;
```

```
k = 2*pi/lambda; %wavenumber
```

```
if mod(MNum-1,2)==0
```

```
kxr = k*sqrt(neff^2-n2^2);
```

```
kxm = k*sqrt(n1^2-neff^2);
```

```
C=0.5*n1*dn*k*(neff^-1)*(((kxm*Width+sin(kxm*Width))/(kxm))*((kxm*Width+sin(kxm*Width))/(2*kxm)+(cos(kxm*0.5*Width)-kxm*
```

```
sin(kxm*0.5*Width))^2/(kxr*(1-kxr)^2))^(-1);
```

```
else
```

```
kxr = k*sqrt(neff^2-n2^2);
```

```
kxm = k*sqrt(n1^2-neff^2);
```

```
C=0.5*n1*dn*k*(neff^-1)*(((kxm*Width-sin(kxm*Width))/(kxm))*((kxm*Width-sin(kxm*Width))/(2*kxm)+(kxm*  
cos(kxm*0.5*Width)+sin(kxm*0.5*Width))^2/(kxr*(1-kxr)^2))^(-1);
```

```
end
```

```
beta = k*neff; dum2 = beta*Periode/pi;
```

```
if (dum2-floor(dum2))>0.5
```

```
NN = floor(dum2)+1;
```

```
else NN = floor(dum2);
```

```
end
```

```
F1=-1/2*i*(-exp(-i*(Periode+space)*pi*-NN/Periode)+exp(i*(-Periode+space)*pi*-NN/Periode))/(pi*-  
NN);
```

```

F2=-1/2*i*(-exp(-i*(Periode+space)*pi*NN/Periode)+exp(i*(-Periode+space)*pi*NN/Periode))/(pi*NN);

F0 = space/(Periode);

C1 = C*F1;

C2 = C*F2;

dbeta = 2*beta-NN*2*pi/Periode;

Q = [(-i*0.5*dbeta-i*C*F0) -i*C1 i*C2 (i*0.5*dbeta+i*C*F0)];

[PP,eg]=eig(Q);

eg1 = eg(1,1);

eg2 = eg(2,2);

M = matE(L,eg1,eg2);

TT = (PP)*M*inv(PP);

r = -(TT(2,1)/TT(2,2));

t = TT(1,1)-TT(1,2)*TT(2,1)/TT(2,2);

if Pil==1 y = r; else y = t; end

```

Mode solver

```

function y=modesolv(nleft,nright,lambda,Width,M)

m = smodes(nleft,nright,lambda,Width); %the number of modes n_l n_r

sol = [];

k=2*pi/lambda;

for p = 1:m

if mod(p-1,2)==0

xl = 0; xu = ((p-1)*0.5*pi+pi/2)-10^-20;

dum = bisection1(nleft,nright,lambda,Width,xu,xl);

sol=[sol, sqrt((k*nleft)^2-(2*dum/Width)^2)/k];

else xl = pi/2; xu = ((p-1)*0.5*pi+pi/2)-10^-20;

dum = bisection2(nleft,nright,lambda,Width,xu,xl);

sol=[sol,sqrt((k*nleft)^2-(2*dum/Width)^2)/k];

```

```
end
```

```
end
```

```
y = sol(M);
```

Bibliography

- [1] Yariv Amnon and Pochi Yeh. *Optical waves in crystal: Propagation and control of laser radiation*. Wiley, Canada, 1994.
- [2] Han Berends. *Integrated Optical Bragg Reflectors as Narrowband Wavelength Filters*. PhD thesis, the University of Twente, P.O. Box 217, 7500 AE Enschede, The Netherlands, 1997.
- [3] OlympIOs Integrated Optics Software C2V. P.O. Box 318, 7500 AH Enschede, The Netherlands. <http://www.c2v.nl/software>.
- [4] Shun-Lien Chuang. A coupled-mode theory for multiwaveguide systems satisfying the reciprocity theorem and power conservation. *J. Lightwave Technol.*, LT-5(1):174–183, 1987.
- [5] D.G. Hall and B.J. Thompson. Selected papers on coupled-mode theory in guided-wave optics. volume MS 84 of *SPIE Milestone Series*. SPIE Optical Engineering Press, Bellingham, Washington USA, 1993.
- [6] M. Hammer. Resonant coupling of dielectric optical waveguides via rectangular microcavities: The coupled guided mode perspective. *Opt. Quantum Electron.*, 214(1), 2002.
- [7] M. Hammer and E.van Groesen. Total multimode reflection at facets of planar high contrast optical waveguides. *J. Lightwave Technol.*, 20(8):1549–1555, 2002.
- [8] M. Hammer and D. Yudistira. Grating assisted rectangular integrated optical microresonator. *Proceedings of ECIO*, 2003.

- [9] M. Hammer, D. Yudistira, and R. Stoffer. Modeling of grating assisted standing wave microresonators for filter applications in integrated optics. to be published, 2003.
- [10] B.E. Little, S.T. Chu, H.A. Haus, J. Foresi, and J.-P. Laine. Microring resonator channel dropping filters. *J. Lightwave Technol.*, 15(6):998–1005, 1997.
- [11] B.E. Little, S.T. Chu, Y. Pan, and W.nad Kokubun. Microring resonator arrays for vlsi photonics. *IEEE Photonics Technol. Lett.*, 12(3):323–325, 2000.
- [12] M Lohmeyer. Mode expansion modeling of rectangular integrated optical microresonators. *Opt. Quantum Electron.*, 34(5):541–557, 2002.
- [13] M. Lohmeyer, N. Bahlmann, O. Zhuromskyy, and P. Hertel. Radiatively coupled waveguide polarization splitter simulated by wave-matching-based coupled mode theory. *Opt. Quantum Electron.*, 31:877–891, 1999.
- [14] C. Manolatou, M.J. Khan, S. Fan, H.A. Haus, and J.D. Joannopoulos. Coupling of modes analysis of resonant channel add-drop filters. *IEEE J. Quantum Electron.*, 35(9):1322–1331, 1999.
- [15] A.I. Nosich and S.V. Boriskina. Fast solution to the scattering by arbitrary smooth dielectric cylinders based on the method of regularisation. *Proceedings of ICTON*, pages 27–30, 2000.
- [16] C. Vassallo. *Optical Waveguide Concepts*. Elsevier, Amsterdam, 1991.
- [17] The Math Works. *The student edition of MATLAB the ultimate computing environment for technical education*. Prentice Hall, 1995. User's Guide.
- [18] Pochi Yeh. *Optical Waves in Layered Media*. Wiley, 1988.
- [19] D. Yudistira. *Reflection of Plane Electromagnetic Waves from a Dielectric Multilayer Stack*. University of Twente, Dept. of Applied Mathematics, 2002. Modeling project.

Acknowledgment

While the actual writing of a graduation thesis usually is the results of days, and sometimes nights, of writing, reading, and rewriting by the author, the content of the thesis is the results of contributions of many. Realising that it may be an impossible task acknowledging each and every one I will make an attempt to do so anyway.

First, many suggestions have been useful to complete this thesis. In particular, I would like to express my deepest appreciation to my daily supervisor Dr. Manfred Hammer for his proper guidance and support. I would like to thank Dr. Hugo Hoekstra and Prof. Brenny van Groesen and Prof. Tjia May On of Institute Teknologi Bandung (ITB) Indonesia for their support. Light Devices Group (LDG) of department of Electrical Engineering at University of Twente that provided me a nice place to work with nice colleagues (Wico, Edwin and Ronald) and the important thing is that they provided computer simulation *Olympios* for my thesis.

Also, I would like to thank to my friends in Master of Science program of Applied Mathematics 2001 in particular to Hala for her advice in..., to my friends in faith Indonesian Moslems community in Enschede, The Netherlands (IMEA), to my beloved friends in PPI Enschede, to my lunch friends Pak Freddy, Pak Henri, David, and Jahja (Yukem), for a warm friendship. Frurthermore, I want to thank to my friends in Calslaan 1 (Calslaan ers) Rayi, Adi, Esther, Iren that provided me a special dinner with the Calslaan family during the past months. It was really unforgettable moments. Also, I would like to address my grateful thank to my best friend Lukmanul Hakim for his support.

Last but not least I want to thank to my family, my mother, my brothers and sister for their support throughout the years.